University of Texas at El Paso
DigitalCommons@UTEP

Open Access Theses & Dissertations

2011-01-01

Determination of Critical Parameters for Solar Probe Plus Shielding

Sergio Rafael Mendez
University of Texas at El Paso, srmendez2@miners.utep.edu

Follow this and additional works at: https://digitalcommons.utep.edu/open_etd

 Part of the Aerospace Engineering Commons, and the Civil Engineering Commons

Recommended Citation
Mendez, Sergio Rafael, "Determination of Critical Parameters for Solar Probe Plus Shielding" (2011). *Open Access Theses & Dissertations*. 2345.
https://digitalcommons.utep.edu/open_etd/2345

This is brought to you for free and open access by DigitalCommons@UTEP. It has been accepted for inclusion in Open Access Theses & Dissertations by an authorized administrator of DigitalCommons@UTEP. For more information, please contact lweber@utep.edu.

DETERMINATION OF CRITICAL PARAMETERS FOR SOLAR PROBE PLUS SHIELDING

SERGIO RAFAEL MENDEZ

Department of Civil Engineering

APPROVED:

Cesar Carrasco, Ph.D., Chair

Carlos M. Ferregut, Ph.D.

Noe Vargas Hernandez, Ph.D.

Benjamin C. Flores, Ph.D.

Interim Dean of the Graduate School

Copyright ©

by

Sergio Rafael Mendez

2011

DEDICATION

I dedicate this thesis and all that I do to my family and to the loving memory of my mother Elvia Ortiz and my beloved grandmother Belia Mendez

DETERMINATION OF CRITICAL PARAMETERS FOR SOLAR PROBE PLUS SHIELDING

by

SERGIO RAFAEL MENDEZ, B.S.C.E.

THESIS

Presented to the Faculty of the Graduate School of

The University of Texas at El Paso

in Partial Fulfillment

of the Requirements

for the Degree of

MASTER OF SCIENCE

Department of Civil Engineering

THE UNIVERSITY OF TEXAS AT EL PASO

December 2011

ACKNOWLEDGEMENTS

I would like to thank Dr. Cesar Carrasco for being my mentor throughout all my studies, both graduate and undergraduate, and for being my thesis committee chairman. A special thanks to Dr. Carlos M. Ferregut and Dr. Noe Vargas Hernandez for being my thesis committee members.

I wish to thank my parents and family for all their love and support throughout all my life, particularly my beloved sister Lizbeth Maynez and her husband Jesus Maynez for giving me a house and most importantly a family when I needed it the most. I want to thank my grandfather Rafael Mendez for always looking out for me, and setting an example of hard work and dedication.

I would like to thank my partner and friend David Ledesma for his true and loyal friendship all these years we have worked together towards the same goals sharing the same vision. I wish to thank all my fellow members of the American Society of Civil Engineers (ASCE), specially the Steel Bridge team for all their hard work throughout these years, and Dr. Shane Walker for his unconditional guidance, kindness and advice.

I would like to extend special gratitude to everyone at Henry K. Ng Consulting Engineers for the opportunity to learn from them, specially Henry K. Ng, Javier Carlin, Edmund Castle, Manuel Levario, and Armando Sanchez.

Finally I want to express my deepest gratitude to my closest friends: Miriam Flores, Alejandra Maynez, Alejandra Marco Chavez, Carlos Chavez, Alejandra Gallegos, Alejandra Rodriguez, Victor Salas, Belen Valdez, Mabel Terminel, Kristian Simental, Marisol Sierra, my

cousin Hugo Mendez, and everyone else who gave me their support and encouragement, and helped to shape me into the man that I am, nothing would have been possible without you guys. Thank You!

ABSTRACT

A methodology to determine critical design parameters such as critical "design" particle size, and critical "design" impact speed for the shielding of the Solar Probe Plus spacecraft was developed in this thesis. Several critical components and surfaces of the spacecraft such as the Solar Array North, the Thermal Protection System, and the ISIS Instruments were analyzed in this study. The methodology determines the critical "design" particle size based on the required reliability or probability of no impact. Current NASA methods do not provide means to calculate critical "design" impact speeds for missions such as Solar Probe Plus, where the distributions of impact speeds can vary significantly from particle size to particle size and with position of the spacecraft as a function of time due to the non-circular orbital trajectory that the spacecraft will follow. Previous methodologies attempted to determine the critical "design" impact speed based on the distribution of speeds from the smallest particle size, and yielded conservative results. This thesis uses the entire distributions of impact speeds for all dust particle sizes in an attempt to reduce conservatism and thus launching and material costs for the mission. This is crucial because it accounts for the dependency of the impact speed distribution on particle size, and is achieved by normalizing the total cumulative number of impacts as a function of the normal component of impact speed for every particle size. Results from this thesis show that the critical impact speed is significantly reduced when compared to previous methodologies. As the required probability of no impact increases, the critical particle size also increases, and the critical impact decreases.

TABLE OF CONTENTS

LIST OF TABLES

LIST OF FIGURES

CHAPTER 1
INTRODUCTION

1.1 General

Solar Probe Plus is one of the most ambitious missions ever conceived by NASA. The objective of Solar Probe Plus is to reach where no one has ever explored before: the atmosphere of the Sun. Solar Probe Plus (SPP) will investigate the dynamics of solar wind and the nature of the heat from the Sun Corona (Johns Hopkins University Applied Physics Laboratory 2008). As the Solar Probe Plus spacecraft approaches the vicinities of the Sun it will be subjected to severe impacts from micrometeoroid particles, not only at high densities but also at very high velocities (Carrasco *et al.* 2006).

The main concerns on the solar probe mission are to maintain the structural components free of penetration or damage due to a one time extreme impact and the erosion that could be caused by large number of impacts of small particles. Therefore a clear understanding of the solar dust environment, as well as the shielding design methodologies is of extreme importance for the successful completion of the ambitious mission. The following sections present the literature review on dust models and shielding concepts considered in this thesis.

1.2 Background on dust models

Several studies have been done in the past to investigate the behavior of micrometeoroid and orbital debris (MMOD) at near sun environments. The following paragraphs present a brief description of the literature research done on interplanetary dust models in chronological order.

Divine (1993) presents a thorough description of an interplanetary meteoroid environment by classifying it into five different groups or populations. Each population has an

independent distribution in terms of particle mass, eccentricity, and perihelion distance. Divine classified the five populations in increasing order of their mean particle size, and named them based on a distinctive characteristic of their distribution. The names of the populations are: eccentric, inclined, halo, core and asteroidal, and their masses range from 10^{-18} g to 1 g.

Ishimoto and Mann (1999) proposed a model to estimate the particle flux and number density distribution of interplanetary particles within 1 astronomical unit (AU) from the sun taking into account both the collision of particles and the Poynting-Robertson effect. According to Ishimoto and Mann, collisional evolution and particle mass distribution depend on the orbits of collision fragments. Ishimoto and Mann showed that the hyperbolic particles known as Beta-Meteoroids that have masses in the ranges of 10E-15 to 10E-13g at 1 AU lead to the supply of masses greater than 10E-7 g within the 1 AU. The destruction of particles and creation of small fragments creates a steeper slope of the particle mass distribution at the inner solar system.

Mann *et al.* (2000) investigated the structure and composition of the near sun dust cloud. They derived a set of trajectories of the dust grains by performing numerical integrations, and obtained the spatial distributions of different dust populations within a distance of 10 solar radii from the sun. They found that simple extrapolation of interplanetary dust cloud into the solar vicinity does not describe the near sun dust cloud precisely, and that the fluxes and time variations of micrometer sized grains depend on both the physical and chemical properties of the dust.

Jackson (2000) investigated the effect of the Poynting-Robertson phenomena on the orbits of the particles traveling near the sun. Jackson stated that solar radiation would cause the particle to change in size due to evaporation, and concluded that the Poynting-Robertson effect

leads to the capture of a set of interstellar grains passing on hyperbolic orbits through the solar system.

Mann *et al.* (2002) discussed possible techniques and methods to observe and detect interstellar dust particles from spacecrafts traveling in interstellar missions. They state that the radial speed at which interstellar probes have to travel is quite advantageous for detection methods that are based on impact of dust, thus allowing obtaining information about the element composition of dust. The study focused on measurements at the heliosphere, and they concluded that the velocity distributions are sensitive to the structure of the heliosphere transition region.

Mann *et al.* (2004) proposed a model that describes the interaction of particles in a near sun environment. This model is valid for low eccentricity orbits with inclinations of less than 30 degrees from the ecliptic plane, and is heavily based on estimations from solar corona observations, models on dynamical and collisional evolution, and from extrapolating values known at 1 AU toward smaller distances. They presented the cumulative fluxes for particle sizes of that size or larger measured at 1AU, as well as a relation for extrapolation distances less than 1AU that depends on radial distance. They also stated that sublimation accounts as the primary source of particle destruction at 0.1AU, and inwards from 10 solar radii dust destruction varies depending on particle size, material composition, and possibly with time, and thus affects the size distribution. Lorentz force and radiation pressures become important as particles travel closer to the sun, as particles can be deflected onto random orbits. They stated that particles greater than 10 μm are weakly affected by the solar cycle magnetic field variation, and thus can be ignored; that the majority of the dust near the sun is in Keplerian, almost circular, near ecliptic orbits; and that the particles drifting towards the sun due to the Poynting-Robertson effect are in orbits with smaller eccentricities. They finally emphasized that future near sun missions and in-

situ measurements are extremely important to understand and address matters such as: indentifying mass distributions and fluxes of dust particles as a function of the distance from the sun; comparing dust amount in bound orbits with those in hyperbolic orbits, and their dependence on mass and distance from the sun; identifying the size limit between Keplerian orbit particles influenced by magnetic field; and finding what are the major elemental compositions and bulk density of the dust particles and their variability as a function of distance from the sun, and how to correlate these parameters to the particle size.

Kocijaf and Klacka (2004) investigated the motion and possible capture of interstellar dust particles into the solar system considering the gravitational force of the sun, the solar electromagnetic radiation and the interplanetary magnetic field. They discovered that the solar electromagnetic radiation plays an important role in the sense that nonspherical particles can be captured and survive with much more ease than spherical particles. They concluded that the nonspherical particles can survive approximately two years in the circumsolar zone of radios of one astronomical unit.

Klocijaf and Klacka (2004) continued their investigation of the capture of arbitrarily shaped particle dust in the solar system. In their studies spherical and nonspherical particles are only captured when moving in the vicinity of the ecliptic plane. They concluded that submicron sized particles could contribute to the density increase of the circumsolar dust cloud.

1.3 Background on shielding concepts

The articles and reports reviewed in the following paragraphs describe several shielding concepts and studies that have been done in order to protect spacecraft from hypervelocity impact environments. Several of the reports and articles presented in chronological order develop on practices adopted by NASA to protect spacecrafts to ensure their mission success. These

practices include developing ballistic limit equations, complying with satisfactory probabilities of no impact and performing risk analysis checks.

Christiansen (1993) developed design and performance equations for the assessment of the vulnerability of spacecrafts from meteoroid and debris impact. He classified the equations in two kinds: the design or sizing, which determines preliminary estimates of thicknesses and weights; and the ballistic limit or performance, which define the impact conditions such as the particle size, the impact velocity, the impact angle and the density to define the maximum protection that a particular shield can provide. He explained that these equations would continue to evolve as new testing techniques and technologies become more advanced and available.

Christiansen *et al.* (1995) presented the study and development of the innovative Stuffed Whipple shield, a low weight shield developed by NASA Johnson Space Center and Marshall Space Flight Center engineers that increases the protection of the conventional Whipple shields. The Whipple Stuffed shield includes a flexible blanket that combines Nextel ceramic fabric cloth and Kevlar stuffing, enclosed between the aluminum bumper and rear wall of a Whipple shield. This shield is most effective when the standoff distances are short. Hypervelocity tests using light gas gun launchers with aluminum projectiles were used to test the shield. CTH hydrocode simulations were also performed and they showed that a shaped charge projectile of hollow cylinder shape at elevated temperature is more damaging than a solid sphere of equal weight at ambient temperature. They also developed corresponding ballistic limit equations.

Christiansen and Kerr (2001) provided several different equations that establish the performance efficiency of meteoroid/orbital debris shield systems for the International Space Station. It should be noted that these semi-empirical relationships were developed after series of hypervelocity impact tests, using light-gas gun launchers with test velocities varying from 2 to 7

km/s. Christiansen and Kerr also state that the equations serve as benchmarks to measure the protection performance versus mass and standoff distance for the development of future shield systems. The ballistic limit equations developed by Christiansen and Kerr assumed that the particles were spherical and homogenous, and provided the particle diameter that caused a shield to fail as a function of the impact conditions, which include impact speed, impact angle and impactor density. The ballistic limit equations were implemented using computer tools such as the BUMPER code, which asses the probability of no penetration for the critical component being shielded.

Hyde *et al.* (2001) described how the BUMPER code has been used extensively in the analysis of meteoroid and orbital debris risk for different space systems. BUMPER requires a finite element model that describes the spacecraft geometry, the location of the systems and subsystems and where the shielding materials are located. They stated that different levels of damage can be assessed for particle components; this depends on the availability of a ballistic limit equation that describes the particle size, impact velocity, angle and density of the damage causing particle. BUMPER code assessment process includes: The Spacecraft Configuration phase, where a finite element model is created, and properties identified; the Geometry phase, where the individual elements of the finite element model are assigned the collision probabilities using different environment models; the Response function, which characterizes the impact resistance properties of the different regions of the spacecraft; and finally the M/OD risk calculations.

Christiansen (2003) developed a very thorough report that described the different steps and considerations that must be observed when designing a shielding system for a spacecraft that would be exposed to hypervelocity impacts during a specific mission. Christiansen described the

meteoroid and debris environments that a spacecraft could be subjected to, and the implications that are to be addressed to protect it, he used the Space Shuttle orbiter as an example. Christiansen then derived a methodology for the assessment of risks and to verify the protection requirements, this methodology included meeting a probability of no penetration as well as different design requirements. He then developed ballistic limit equations based on the results of hypervelocity tests; implemented a low-weight shield, and used the software to evaluate the BUMPER Code. Christiansen developed several techniques used to select the shielding configuration necessary to protect the spacecraft, several shields such as Whipple stuffed, multi shock, and regular Whipple shield were investigated. Finally he proposed different recommendations for future designers as well as explained that the two major objectives of the report were to develop low weight and effective shielding methods to protect spacecraft from meteoroid and impact debris, as well as to develop design and performance equations to allow the implementation of conventional shielding and enhanced shielding for spacecraft protection.

Christiansen *et al.* (2009) presented the methods and shielding configurations implemented to protect the International Space Station (ISS) from micrometeoroid and orbital debris impact. They explained that one of the primary objectives of the study was to compare the damage observed on ISS returned hardware to that predicted by the BUMPER Code Risk Assessment program. They concluded that the ISS protection would be improved once the protection of specific areas such as the service module area is augmented, and that the observed damage on hardware was in fact accurately predicted by BUMPER.

Ryan *et al.* (2010) studied the results of hypervelocity impact tests performed on aluminum alloy Whipple shields to understand the failure mechanics in what is known as the shatter regime. They found out that a ballistic limit curve provided a more accurate reproduction

of the shield behavior than the ballistic limit equation. Linear interpolation done by the ballistic limit equations in the shatter regime was not representative and did not agree with the results obtained by the hypervelocity tests. They concluded that further investigation is necessary to determine if the linear interpolation can be replaced in the shatter regime.

Ryan and Christiansen (2011) developed a software program that performs ballistic limit equations for commonly used spacecraft structures that are prone to hypervelocity impacts of micrometeoroid debris. The software is divided in two modules: the design module, which is the one that calculates the preliminary dimensions of the shield configuration given a design particle size; the performance module performs a more detailed shielding analysis which reports the particle size that would be stopped given a shielding configuration.

1.4 Objective

Most of the work done in relation to spacecraft shielding structures has focused on low-earth orbit (LEO) missions. The concept of Probability of No Impact (PNI), discussed in detail later, has been widely accepted as a metric used to define a "design" particle size for the design of shielding structures. If a shield is designed to stop the "design" particle, then its "probability of failure" is one minus the PNI. However, the concept of the PNI, as currently used, does not provide any insight into what impact speed to use for design purposes. For low earth orbit (LEO) missions where the velocity distributions are quite narrow because of the close to circular orbits of the particles and spacecraft, the selection of an impact speed is not problematic. However Solar Probe will not follow a circular orbit and this will create a significantly wider distribution of impact velocities, which makes the selection of a "design" impact speed difficult.

This thesis proposes the extension of the concept of the PNI to also address the selection of the impact speed for interplanetary missions where the impacts speed can vary significantly over the duration of the mission. A first attempt at addressing the selection of an impact speed was developed by using the impact speed distribution of the smallest particle, which tends to be significantly higher than that of larger particles. The methodology used required Monte Carlo simulations to be conducted by selecting pairs of impact speeds and particle masses from the cumulative number of impacts as function of particle size and the impact speed cumulative density function for the smallest particle. While this allowed us to select an impact speed, it was understood from the beginning that it could be significantly conservative. For this reason a more detailed methodology was also developed which accounts for the complete impact velocity distribution as a function of the particle size.

CHAPTER 2
DUST PARTICLE MODEL

2.1 General

The interplanetary model used for the scope of this thesis is described in this chapter. The model was developed by Mann *et al*. (2004), and it presents the calculation of the cumulative fluxes and density numbers of dust particle populations based on the current knowledge of near-solar dust environment. The theory and history on the development of this model are described in the following sections. Section 2.1 describes the sources of dust population and how the dust population is distributed. Section 2.2 presents the flux model that is valid for circular and low inclination orbits. Section 2.3 describes the dust behavior model at high latitudes. The effects of dust particles collisions, as well as other mechanisms that contribute to particle destruction, and their effect on flux models are presented in section 2.4.

2.2 Sources of dust environment population

Several efforts to measure the density and properties of dust near the sun have been performed over the years. Some of these measurements include the F-corona and zodiacal light observations, which have led to identify particles that range in the sizes of 1 to 100 μm, corresponding to masses ranging from 10^{-11} g to 10^{-5} g. Another research effort consisted of in-situ measurements, which include in space and meteor observations of particles that enter the Earth's atmosphere, in contrast with the F-corona and zodiacal light observations, the in-situ observations often detect particles considerably smaller than several micrometers. The majority of the dust particle population is produced by the breakup of comet and asteroid fragments, and

by the comet and asteroids themselves. Only a small portion of the interstellar dust contributes to the environment inside 1 Astronomical Unit (AU), therefore the model focuses on comets and asteroids, as well as their contribution to the particle population. The Poynting Robertson effect and the Lorentz force are of special interest since the first one increases the dust number density as the solar distance decreases, while the latter deflects charged particles away from their orbits. The number density can be assumed to increase inversely proportional to r^{-1}, where r is the distance from the sun (Mann *et al.* 2004).

2.3 Dust environment model at low latitudes

The following model described in Mann *et al.* (2004) was developed on the assumptions that dust particles follow low inclination orbits, merely less than 30°. The cumulative flux of dust of masses greater than m at r_o=1AU is given as:

$$F(m, r_0) = (c_1 m^{g1} + c_2)^{g2} + c_3(m + c_4 m^{g3} + c_5 m^{g4})^{g5} + c_6(m + c_7 m^{g6})^{g7} \quad (1)$$

With c_1=2.2x10³, c_2=15, c_3=1.3x10^{-9}, c_4=10^{11}, c_5=10^{27}, c_6=1.3x10^{-16}, c_7=10^{6}, g_1=0.306, g_2=-4.38, g_3=2, g_4=4, g_5=-0.36, g_6=2, g_7=-0.85, where F(m,r_o) is given in units of m^{-2}s^{-1}.

The cumulative spatial density or density number for an isotropic flux is given as:

$$N(m, r) = \frac{4F(m,r)}{v(r)} \quad (2)$$

Where v(r) is the average impact velocity, which can be defined as:

$$v(r) = v_0(\frac{r}{r_0})^{-0.5} \quad (3)$$

Where V_o=20 km s^{-1}, and is the average impact speed at r_o=1AU. For radii that are located within 1 AU the cumulative flux is equal to:

$$F(m, r) = F(m, r_0)(\frac{r}{r_0})^{-1.5} \quad (4)$$

The increase on cumulative flux is proportional to $r^{-1.5}$ for particles following nearly circular orbits and under the drag of the Poynting Robertson effect. Traveling at the same speeds, 5% of the flux follows retrograde orbits.

2.4 Dust environment at high latitudes

For particles traveling at high inclination orbits, which are orbits at more than 30° inclinations, the cumulative spatial density at 1 AU can be assumed to be 10% of that at the ecliptic for particles smaller than 5μm, and 5% for particles greater than 5 μm. The extrapolation of the number density at different radii is steeper than that close to the ecliptic, and is proportional to $r^{-1.5}$. Traveling at the same speed, 50% of the flux follows retrograde orbits and the other half follows prograde orbits.

2.5 Mechanisms that contribute to dust destruction

Collision between particles and sublimation are phenomena that can significantly affect the size distribution of particles and must be incorporated in the dust environment models. Figure 2.1 shows particle fluxes at 0.1 AU near the ecliptic based on different assumptions, for instance the solid line represents the distribution derived by equations (1) through (4) which does not include collision effects; collision model "a" represents a distribution taking into account collision effects and an increasing mass supply from 1 to 0.5 AU and then a constant supply inside of 1 AU; collision model "b" takes into account a constant mass supply from 1 AU inwards; and collision model "c" considers a constant supply of mass only from 1 to 0.5 AU. The mutual collision of particles causes the number of bigger particles, which have mass $m>10^{-7}$ g, to

be reduced significantly because of fragmentation. The smaller fragments are eliminated by radiation pressure which causes a reduction of particles of masses m between 10^{-14} g and 10^{-12} g and can be seen in Figure 2.1.

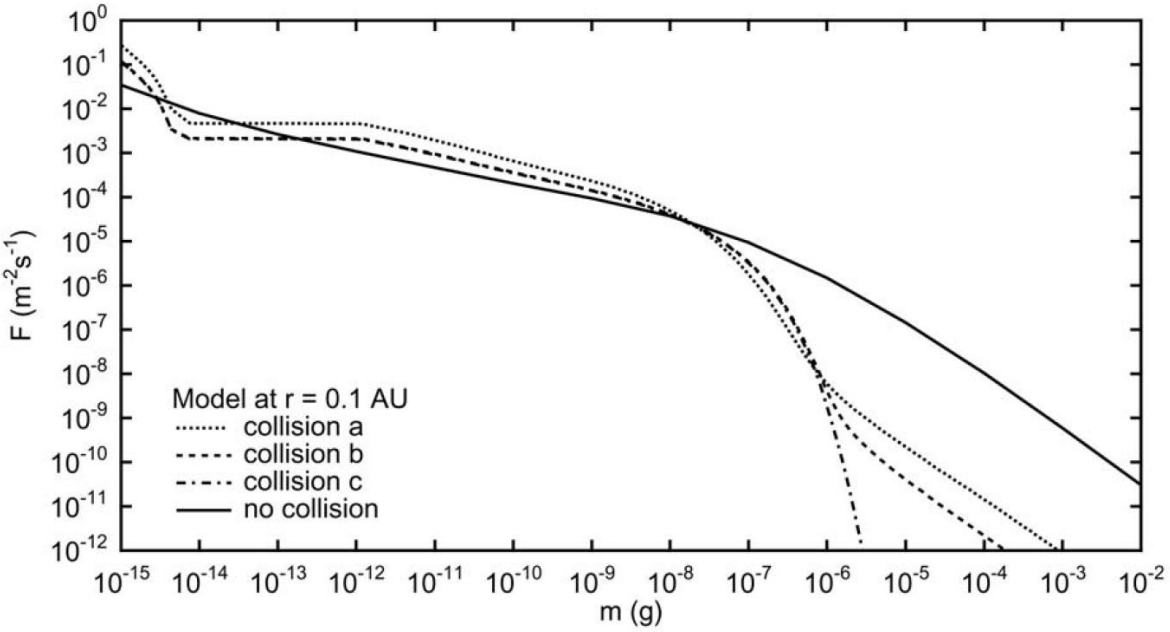

Figure 2.1.- The flux of dust at 0.1 AU near the ecliptic (Mann *et al.* 2004)

Sublimation, rotational bursting of grains and erosion by solar winds destroy particles within 0.1 AU or 20 solar radii around the sun. Depending on the dust particle size and the material composition the destruction of dust happens proportionally with heliocentric distance, as well as possibly with time (Mann *et al.* 2004). Table 2.1 presents the results of several research efforts presented at Mann *et al.* (2004), and shows the zone of sublimation for different material compositions. As can be seen from this table, most of the materials begin to sublimate once the dust particles are inside of 20 solar radii possibly leading to a dust free zone inside of 4-5 solar radii.

Table 2.1- Zone of sublimations for different materials (Mann *et al.* 2004).

Material	Sphere	Fluffy	Ref.
Quartz	1.5–4 $R_\odot$	—	1,2,3
FeO-poor obsidian	1.9–7 $R_\odot$	2.5–3 $R_\odot$	4,5,6,7,8,9,10
FeO-rich obsidian	2.9–6 $R_\odot$	—	5,8
Glassy carbon	4 $R_\odot$	4 $R_\odot$	9,10
Graphite	$\leq$ 5 $R_\odot$	$\leq$ 2 $R_\odot$	2,5,7,8,11
Crystalline Mg-rich pyroxene	5 $R_\odot$	5 $R_\odot$	12
Amorphous Mg-rich pyroxene	5.5–6.5 $R_\odot$	5–6.5 $R_\odot$	12
Basalt	6 $R_\odot$	—	8
Andesite	9–10.5 $R_\odot$	—	3,4,11
Crystalline Mg-rich olivine	10 $R_\odot$	9.5–11 $R_\odot$	12
Amorphous Mg-rich olivine	13.5–15.5 $R_\odot$	12–15 $R_\odot$	12
Astronomical silicate	14 $R_\odot$	—	8
Iron	11–24.3 $R_\odot$	—	3,4
Magnetite	10–40 $R_\odot$	—	6
Water ice	1–2.8 AU	—	2,3,6

References. — (1) Over (1958); (2) Mukai and Mukai (1973); (3) Lamy (1974b); (4) Lamy (1974a); (5) Mukai and Yamamoto (1979); (6) Mukai and Schwehm (1981); (7) Mann *et al.* (1994); (8) Shestakova and Tambovtseva (1995); (9) Kimura, Ishimoto, and Mukai (1997); (10) Krivov, Kimura, and Mann (1998); (11) Mukai *et al.* (1974); (12) Kimura *et al.* (2002).

CHAPTER 3
DUST SHIELDING AND PROTECTION

3.1 General Background and Introduction

Once the dust environment has been established, studied and characterized, the risk of micrometeoroid and orbital debris (MMOD) impact must be addressed by providing necessary dust shielding and protection. An efficient shielding and protection design will help to ensure that the interplanetary mission can be completed successfully. This chapter presents the methodology that has been adopted by NASA to protect spacecrafts from MMOD.

The duration of the mission, as well as the spacecraft size proportionally increase the risk of MMOD impact. The concepts of probability of no failure, or the minimum reliability, are often the base to define the required level of protection against MMOD impact for the specific components of the spacecraft. As the probability of no failure increases, so does the required level of protection, the shielding requirements and weight, this last one usually exponentially (Christiansen *et al.* 2009). As discussed in chapter 2, the model of the dust environment is one of the most crucial parts of the risk assessment, for it will determine the critical particle size and the critical impact speed for the dust particle distributions that the spacecraft will encounter throughout the entire length of the mission.

The maximum allowable level of damage must be clearly identified in order to define the risks and the best alternatives to counter act the risks. The designer can optimize the weight of the shield in the most mass-effective manner by identifying the possible modes of failure and vulnerable areas of the spacecraft components when subjected to MMOD (Christiansen *et al.* 2009).

3.2 Shielding and Protection Design Process and Critical Particle Size Selection

The process that NASA has used to design the shielding and protection for particular components of a spacecraft for low earth orbit (LEO) missions is shown in Figure 3.1

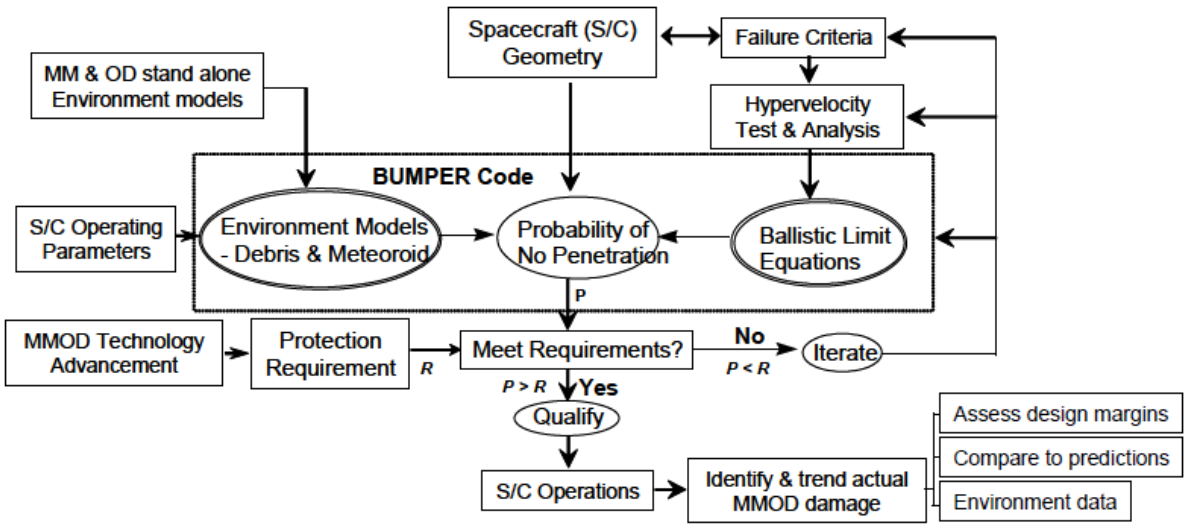

Figure 3.1.- Process to design and evaluate MMOD protection (Christiansen *et al.* 2009)

NASA uses the approach shown in Figure 3.1 as an iterative process, in which preliminary designs already exist and are optimized to meet requirements for protection while keeping mass and volume as low as possible. The first step in the analysis is to determine the spacecraft geometry and shape. The geometry model will include in the end all the different shielding configurations used on the spacecraft. To define the failure criteria, the maximum acceptable damage limit that the specific component being studied can sustain must be quantified. Redundancy is often used to ensure that if a particular component of the spacecraft fails, the rest of the spacecraft can still function for the rest of the mission (Christiansen *et al.* 2009). The failure criteria for the Solar Probe Plus spacecraft is defined as a full penetration or spall of the shield.

BUMPER Code as shown in Figure 3.1 has been used by NASA to perform the risk assessment of spacecrafts since the early 1990's. The missions where BUMPER has been implemented include the International Space Station, the Space Shuttle, and the MIR, among others. BUMPER combines ballistic limit equations with MMOD environmental models to assess risk. The code calculates the number of MMOD particles that exceed the ballistic limit for every element of a finite element model of the spacecraft. This data is used as the total number of failures, and is used to evaluate risk. BUMPER is also capable of determining the relative MMOD risk as a function of obliquity and impact speed, which can help to prepare proper hypervelocity impact tests (Christiansen *et al*, 2003 and 2009).

The requirements to protect a spacecraft from MMOD impact have been usually expressed in terms of the minimum reliability level, that is, the probability of no impact by a particle that will penetrate the shielding configuration, or cause enough damage to jeopardize the success of the mission (Christiansen *et al*. 2009). The Probability of No Impact (PNI) concept must be assessed in terms of the duration of the entire mission. The PNI concept has been accepted as the mean to calculate the critical "design" particle size; however it does not provide a method to select a critical impact speed. An approach in attempting to select a critical "design" speed will be discussed in chapter four. The critical particle of mass "m" that has an acceptable probability of no impact (PNI) defines the structural shield design for that specific component. The shield must be designed so that the critical particle having a probability of no penetration equal to 1-PNI does not penetrate nor causes spall. The probability of having number of impacts equal to *n* of a particular mass or larger is defined by the following Poisson's distribution:

$$P(m,n) = \frac{(N_T(m))^n}{n!} e^{-N_T(m)} \qquad (5)$$

Where N_T is the total cumulative number of impacts for a specific mass "*m*". The probability of no impact (PNI) requires for *n* to be equal to 0, when this condition is met, PNI is equal to P and defined as:

$$PNI = e^{-N_T(m)} \quad (6)$$

Therefore the critical particle size for an acceptable PNI=PNI_A is defined as the particle with a cumulative number of impacts defined as:

$$N_T(m) = -lnPNI_A \quad (7)$$

This process deviates for Solar Probe Plus when assessing impact speeds because of the noncircular orbits which Solar Probe Plus must travel. These orbits will produce a wider distribution of speeds, and therefore the selection of critical impact speed is challenging.

3.3 Typical Shielding and Ballistic Limit Equations

One of the first shield designs proposed for spacecraft protection was the Whipple shield proposed in the 1940's by Fred Whipple. The Whipple, shown in Figure 3.2, shield is composed of a thin bumper, which function is to break up the projectile into a cloud material; and a rear wall, which must be thick enough to resist the blast loading from the debris cloud. The Whipple shield is quite advantageous in the fact that it is far lighter than a single plate shield, which requires the kinetic energy to be dissipated in a very small area. A disadvantage of the Whipple Shield compared to the single wall plate shield is the requirement for more volume due to the standoff distances between the rear wall and the bumper (Christiansen *et al*. 2009).

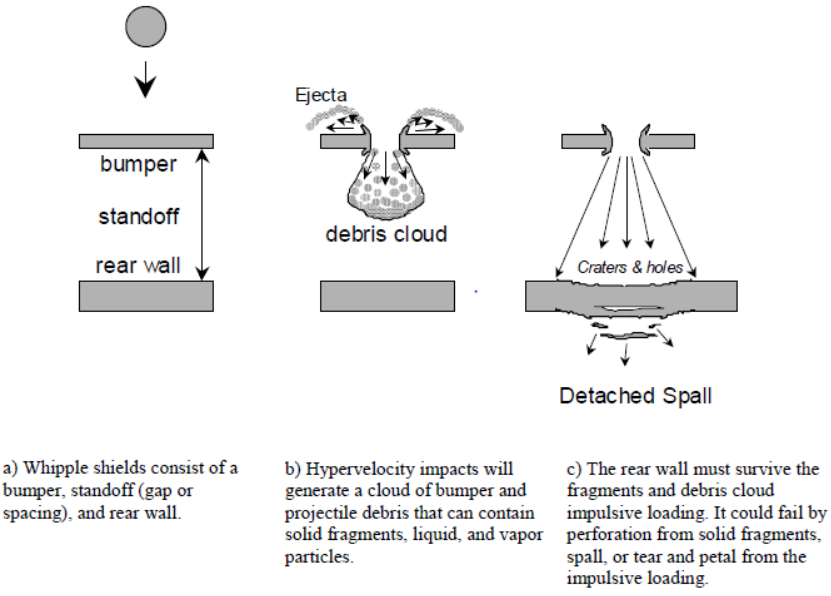

Figure 3.2.-Whipple Shield Schematic (Christiansen *et al*. 2009)

An important consideration to comprehend the performance of spaced shields such as the Whipple shield is to understand the physics of the debris cloud generated after the hypervelocity impact. This cloud can contain a mixture of solid, liquid and vapor materials resulting from the collision between the particle and the bumper. The solid fragments are more damaging as they come in contact with the rear wall of the shield. As projectile velocity, density of the projectile, and density of target increases, as well as the impact becomes more normal, the impact pressure also increases. The shockwave effect after particle and target collisions is a very complex problem. The bumper is compressed by the initial impact shockwaves to high densities and high temperatures, and spall plates will occur if the tensile strength of the material is exceeded. Internal energies and temperature could reach melting or vaporization levels as well (Christiansen *et al*. 2009).

Ballistic limit equations (BLE) are developed from hypervelocity impact (HVI) tests and analysis; many of them are purely empirical based on the data from simulations, analytical

models and impact tests. Hypervelocity tests do not only serve as the base to derive ballistic limit equations, but also to establish the material behavior to hypervelocity impact conditions, and to validate the results of numerical simulations. The tests are performed by accelerating projectiles up to 7 km/s using two-stage light gas guns, however the light gas gun velocity capabilities are very limited compared to the velocity ranges present in the MMOD environment. The objective of the ballistic limit equations is to define the impact conditions such as dust particle size and density, angle, and the impact speed that will cause the shielding configuration to fail. The ballistic limit equations can be classified in two categories, the design, and the performance types. The design equations determine the dimensions and geometry of the shielding configuration, this include the thickness, standoff distances, etc, given a particle size, impact speed and angle of impact; the performance equations relate the particle size on the level or point of failure of a shield configuration to the impact and shield protection parameters (Christiansen *et al*. 2009).

The following is the performance equation that describes the capabilities of the limits of the Whipple shield in terms of the critical particle size that fails the shield by detached spall or full penetration. An important assumption by the performance equations is that the bumper is thick enough to disrupt the high velocity projectiles. For normal impact velocities greater than 7 km/s the critical particle size is defined as:

$$d_c = 3.918 t_w^{\frac{2}{3}} \rho_p^{-\frac{1}{3}} \rho_b^{-\frac{1}{9}} (V cos\theta)^{-2/3} S^{1/3} (\frac{\sigma}{70})^{1/3} \quad (8)$$

Where d_c=critical particle size (cm), t_w = rear wall thickness (cm), ρ_p = projectile density (g/cm³), ρ_b = bumper density (g/cm³), S = overall spacing between outer bumper and rear wall (cm), V = projectile velocity (km/sec), and σ = rear wall yield stress (ksi) (Christiansen *et al*. 2009). Note that when θ=0 degrees, V$\cos\theta$=V_n. Equation 8 shows that the

performance of a Whipple shield is inversely proportional to the square of the normal impact speed for a given particle size. The penetration or level of damage is proportional to the kinetic energy.

CHAPTER 4

DUST-RISK ASSESSMENT FOR SOLAR PROBE PLUS

4.1 Introduction and General Mission Description

Solar Probe Plus will be one of the most historical space missions ever to occur within the next years. The principal objectives of the mission are for the spacecraft to investigate the processes that heat the solar corona and accelerate solar wind. After the lunch has taken place, which is scheduled to be not earlier than 2015, or later than the year 2018, Solar Probe Plus will orbit around the sun twenty four times using seven Venus flybys over a period close to seven years. As shown in figure 4.1, the spacecraft will approach the Sun corona as close as 9.5 Solar Radii, this will happen for at least 88 hours. Within this distance, Solar Probe Plus will travel at speeds close to 125 miles per second, and will have to withstand temperatures close to 2600° Fahrenheit (Johns Hopkins University Applied Physics Laboratory 2008).

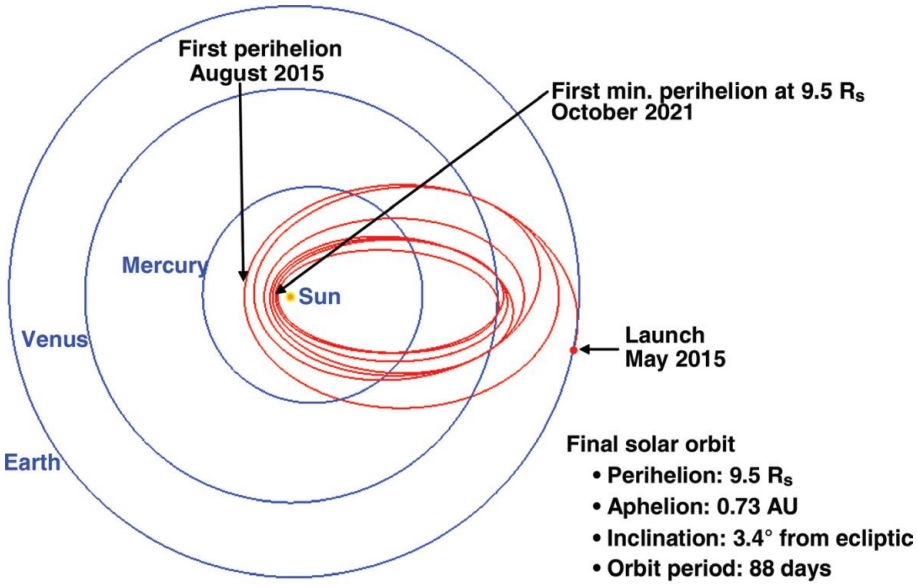

Figure 4.1– Solar Probe Plus mission trajectory (NASA/Johns Hopkins University Applied Physics Laboratory)

NASA has selected five scientific investigations to be conducted using instruments installed in the Solar Probe Plus spacecraft. The Solar Wind Electrons Alphas and Photons (SWEAP) investigation will count and identify the properties of the most abundant particles in the solar wind; the Wide-Field Imager is a telescope that will make three-dimensional images of the solar corona, and of clouds and shocks passing the spacecraft; the Fields Experiment will directly measure the magnetic and electric fields, radio emissions and shock waves that happened at the sun's atmospheric plasma; The Integrated Science Investigation of the Sun (ISIS) will use two instruments that will survey elements in the atmosphere of the Sun using a mass spectrometer to sort ions within the whereabouts of Solar Probe Plus; and the Heliospheric Origins with Solar Probe Plus, which will provide an independent assessment of the scientific performance of Solar Probe Plus (NASA/Johns Hopkins University Applied Physics Laboratory 2010)

4.2 Solar Probe Plus Geometry

Solar Probe Plus is a three axis stabilized, 1350 lb in weight, solar powered spacecraft that will be designed and developed by the Johns Hopkins University Applied Physics Laboratory. The spacecraft includes a hexagonal bus system module with a central propellant tank, and a cylindrical adapter to accommodate the instruments and spacecraft subsystems. The bus also handles the launch loads. To protect the spacecraft bus and instruments, Solar Probe Plus includes a Thermal Protection System composed of an 8 foot diameter, 4.5 inch thick carbon-foam, low conductivity and density solar shield. The spacecraft will be powered by two sets of photovoltaic solar arrays. The primary solar arrays open up when the spacecraft is more than 0.25 AU from the sun, and they retract as the Solar Probe Plus travels closer to the Sun.

Two smaller solar arrays that tolerate higher temperatures are used within the 0.25 AU distance. These arrays are cooled by a pumped liquid system and are protected by the TPS as the spacecraft approaches closer distances towards the Sun. An X/KA-band telecommunications system will provide a high speed downlink through a high gain antenna at distances greater than 0.25 AU from the Sun. For closest approaches the spacecraft will utilize a low speed command uplink through low gain antennas (Johns Hopkins University Applied Physics Laboratory 2008).

Solar Probe Plus is equipped with critical in situ measurement instruments for the success of the mission such as the Fast Ion Analyzer (FIA), the Fast Electron Analyzer (FEA), and the Ion Composition Analyzer (ICA), which are mounted in the forward facing face of the spacecraft and are expected to receive a substantial amount of impacts. The Data Processing Unit (DPU), which is located at the back of the spacecraft, is the largest instrument box, and because of its large area it is a high impact area of Solar Probe Plus. Figure 4.3 shows the schematic for the spacecraft.

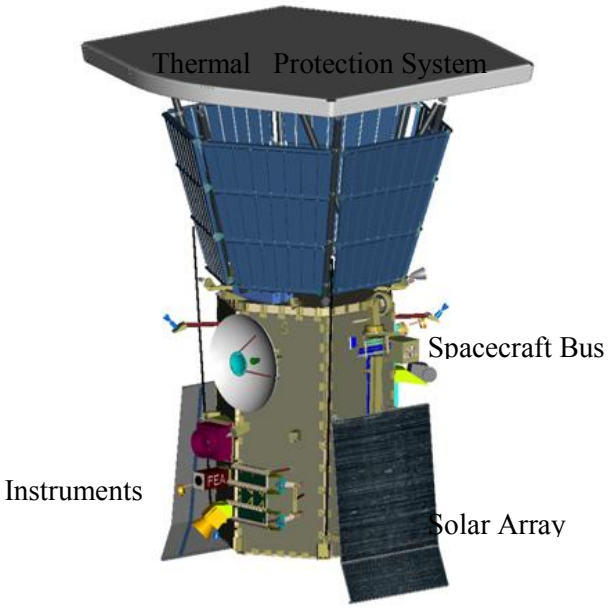

Figure 4.2.- Solar Probe Plus geometry (NASA/Johns Hopkins University Applied Physics Laboratory)

4.3 Methodology

As it has been discussed throughout this thesis, the Solar Probe Plus spacecraft will encounter a hazardous dust environment. Smaller particles will present risk of damages to instruments, cables, optics and thermal surfaces, while the bigger particles present a risk to larger structural components and boxes. To calculate the critical parameters for any specific component a modified concept of Probability of No Impact was used, and the total cumulative number of impacts as a function of particle mass, impact angle and speed over the entire mission had to be calculated.

A MATLAB code was developed to integrate the impacts over the entire trajectory time as Solar Probe Plus orbits around the sun. The total number of impacts for a particle of mass m or larger over a specific surface of area A is defined as:

$$N_T(m) = \frac{A}{4}\int_{\Gamma} N(m,|\mathbf{r}(t)|)\,\mathbf{v}(t)\cdot\mathbf{n}(t)dt \qquad for\ \ \mathbf{v}(t)\cdot\mathbf{n}(t) > 0 \tag{9}$$

Where N(m,|r(t)|) is the cumulative dust density defined by equations (1) through (4) in chapter 2 and section 2.3. r(t) is the norm of the spacecraft position vector as a function of time; v(t) is the relative dust velocity vector with respect to the spacecraft; and n(t) is the unit vector normal to the surface being considered and pointing inward to the component being studied. Both the relative velocity and normal unit vectors are a function of time, and the integration is done on the orbit Γ traced by r(t). This integral does not have a close form solution and was solved numerically. The statistics on impact angle and impact speed were collected at every time step in the integration process. For this thesis three Solar Probe Plus spacecraft components were analyzed using this procedure: The solar arrays, the thermal protection system, and the ISIS

instruments. For irregular surfaces such as the ISIS instruments, the structure was divided into several surfaces for the calculation of the integral, thus requiring several hours of computation time.

The integration was carried out three different times for the three components discussed in order to compare the results of the critical parameters for three different cases. The first case used a previous methodology developed at the University of Texas at El Paso in earlier research efforts that produced very conservative results for critical impact speeds, this methodology uses collision model "a" from Mann *et al*. 2004 discussed in chapter 2 and the impact speed distribution of the smallest particles (conservative approach); the second case considers the methodology proposed in this thesis that reduces the conservatism of the previous methodology by taking into account the entire impact velocity distribution as a function of the dust particle size and also considering collision model "a" from Mann *et al* 2004; and the third one also uses the new methodology, however it neglects any collision effects.

The previous methodology to select critical parameters is outlined as follows and is applied to every spacecraft component of interest:

1) Plots of the cumulative number of impacts as a function of particle size and impact speeds are obtained from the numerical integration of the flux density.
2) A histogram of the number of impacts as a function of impact speed and impact angle is developed for the smallest dust particle.
3) The histogram is reduced by calculating the normal impact speeds, thus eliminating the obliquity angle from the histogram.
4) The data is transformed into a cumulative density function (CDF) and a probability density function (PDF).

5) A Monte Carlo simulation is conducted by selecting pairs of particle masses and impact speeds from the cumulative number of impacts as function of particle size CDF and the impact speed CDF respectively. Then, a CDF of the kinetic energy distribution of the MC samples is generated.
6) The critical impact energy is calculated from the Monte Carlo pairs as the one corresponding to the selected probability of no impact. The critical particle size is selected from the mass CDF as the one that meets a required probability of no impact (PNI). The critical normal impact speed is then calculated from the critical particle mass and the critical impact energy.

The new methodology attempts to consider the dependency of the impact velocities distributions on dust particle sizes. This is done by the following process:

1) Plots of the cumulative number of impacts as a function of particle size and impact speeds are obtained from the numerical integration of the flux density.
2) A histogram of the number of impacts as a function of impact speed and impact angle is developed for all dust particles
3) The histogram is reduced by calculating the normal impact speeds, thus eliminating the obliquity angle from the histogram.
4) A cumulative density surface as a function of dust particle size and normal impact speeds is generated by normalizing the number of impacts as a function of impact speed for all particle sizes.
5) A Monte Carlo simulation is conducted by selecting pairs of particle masses and impact speeds from the cumulative density surface generated in step 4. This requires a double interpolation performed by a software tool. Then, a CDF of the kinetic energy distribution of the MC samples is generated.

6) The critical impact energy is calculated from the Monte Carlo pairs as the one corresponding to the selected probability of no impact. The critical particle size is selected from the mass CDF as the one that meets a required probability of no impact (PNI). The critical normal impact speed is then calculated from the critical particle mass and the critical impact energy.

As discussed in the description of the methodologies, it is the normal impact speeds that are used in the Monte Carlo simulations. This is because experiments have shown that the level of damage generated by hypervelocity impacts is proportional to the normal component of the velocity vector.

4.4 Typical Results: Solar Array North

In this section the typical results of an integration computation are presented. The component selected for this section is the Solar Array North, and the results correspond to the collision model "a" from Mann *et al* 2004 using the new methodology discussed previously. To analyze the impact risks on the Solar Array North, the surface was divided into discrete sections for the integration to be performed. The seven different sections considered are the Primary North Side a, Primary North Side b, Secondary North Side a, Secondary North side b, Primary North, Primary South and Solar Array North All Sides. Figure 4.3 shows the location of the Primary North Side a and Secondary North Side a, Primary North Side b, and Secondary North Side b are on the opposite side of side a. Primary North comprises both sides a and b of Primary North arrays, and Secondary North includes both sides a and b of the Secondary North array.

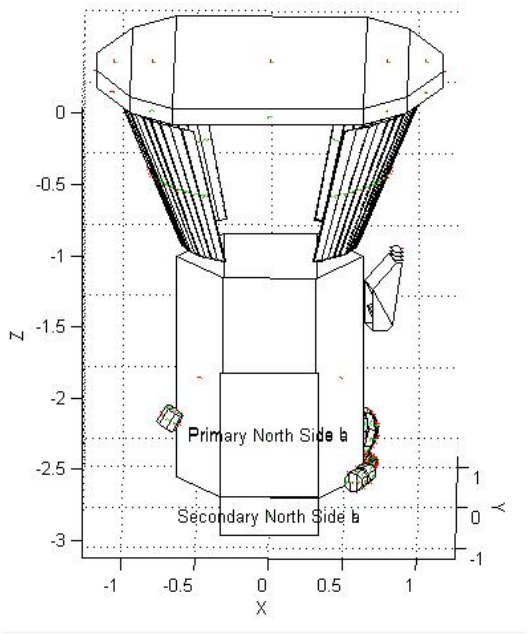

Figure 4.3. - Location of discretized surfaces for Solar Array North

Figure 4.4 illustrates the total number of impacts on Solar Array North for a particle of 424.3138 μm or a weight of 0.0001 grams, and figure 4.5 presents the total number of impacts as a function of particle diameter for all different discrete surfaces defined before. It can be seen on both figure 4.4 and 4.5 that the larger the area, the larger the number of total impacts, as Primary North arrays experience more impact activity than Secondary North arrays. Figure 4.5 also proves that the combination of all the surfaces will have a greater number of impacts as a function of the particle size, and shows how some surfaces receive less impact due to shadowing, which is the protection from impact created by the positioning of other surfaces of the spacecraft.

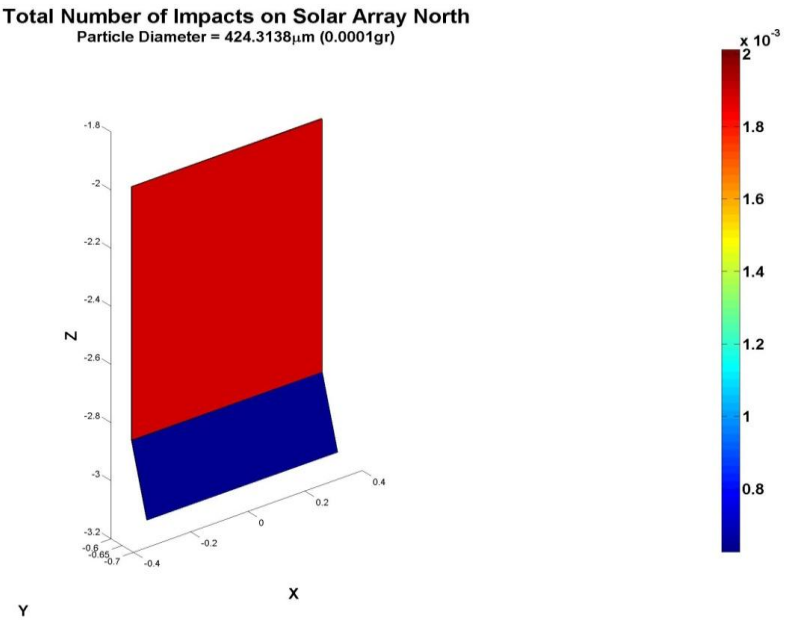

Figure 4.4. - Total number of impacts on Solar Array North

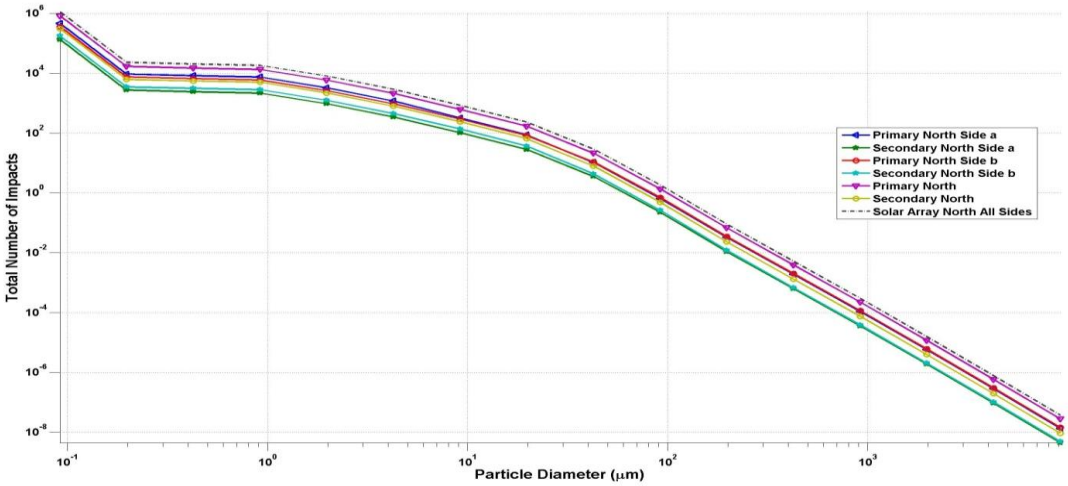

Figure 4.5. - Total number of impacts as a function of particle diameter for Solar Array North (Using collision model "a" from Mann *et al*. 2004)

Figure 4.6 shows the flux of particles with a diameter of 424.3138 μm as a function of time. From figure 4.6 it can be seen that there are certain patters for the particle fluxes for certain ranges of times. The "peaks and valleys" are due to the location of the spacecraft as a function of time. The highest fluxes occur when the spacecraft is at closer distances to the Sun, and the

opposite happens for the valleys. As expected the combination of all the surfaces areas represent once again the largest concentration of particle fluxes, with the Primary North arrays being the greatest contributor.

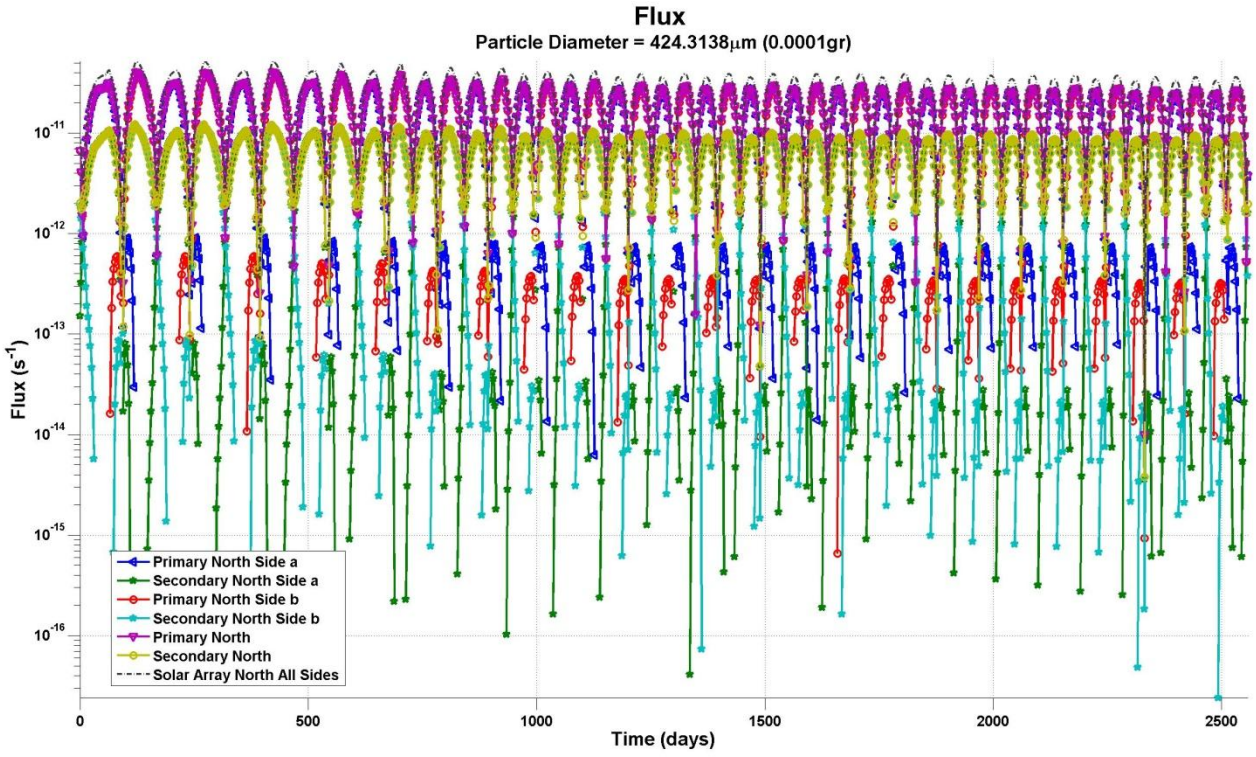

Figure 4.6. - Particle flux as a function of time for Solar Array North

Figure 4.7 shows the normalized number of impacts transformed into a cumulative density function for the Primary North Side "a" array as a function of both particle size and normal impact speed. From this graph Monte Carlo samples can be obtained to lead to the calculation of critical parameters corresponding to the required probabilities of no impact as discussed in the description of the methodologies above. Figure 4.7 shows that as the particle size becomes smaller, the distribution of normal impact speeds widens, and higher normal

impact speeds are more likely to occur than when the particle size is bigger. As particle size increases, the normal impact velocities are mostly distributed over smaller impact speeds. This is the reason why the new methodology reduces conservatism in the critical parameters calculation.

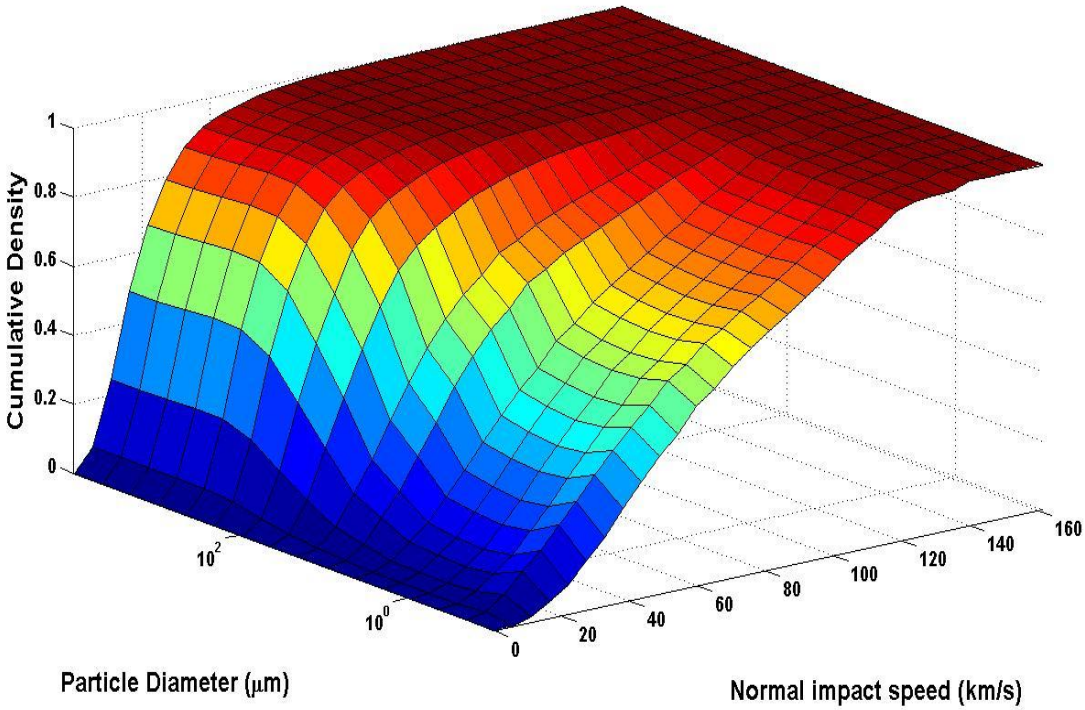

Figure 4.7. - Cumulative density as function of both particle diameter and normal impact speed

Figure 4.8 shows the results of the critical particle size as a function of the corresponding probability of no impact. Primary North both sides "a" and "b" have the largest particle sizes for the required probability of no impact, this is because they have the largest surface area of Solar Array North. Secondary North "a" and "b" have similar particle sizes as well, but their results are smaller than Primary North because they have smaller areas. The curves shown in figure 4.8 have a well defined shape and are translated in the vertical direction depending on the surface being studied.

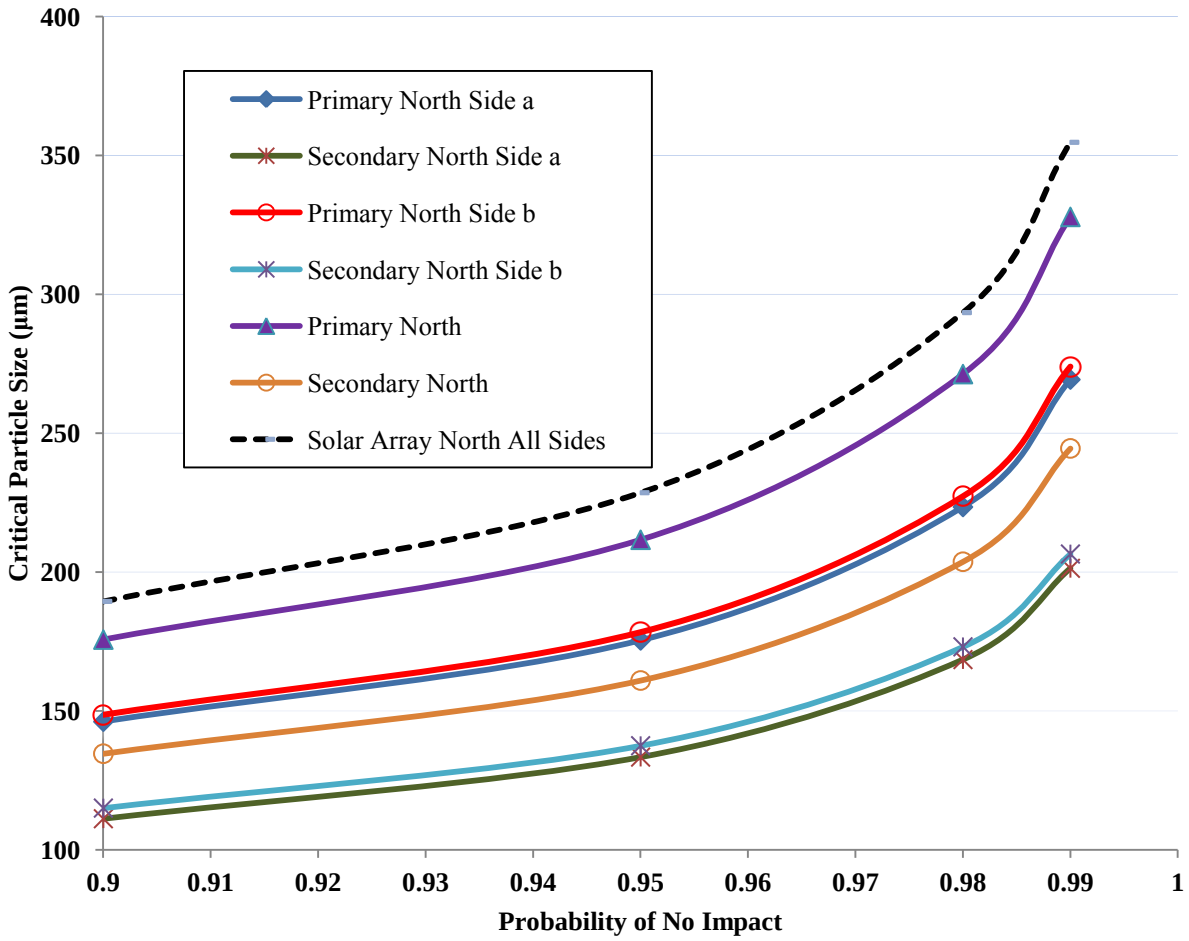

Figure 4.8. - Critical Particle size as function of Probability of No Impact

Figure 4.9 presents the critical impact speed as a function of probability of no impact for all the surfaces where the integration was carried out. Secondary North side "b" resulted with the highest normal impact speeds. The curves in Figure 4.9 are very well defined as well, and are only translated vertically depending on the surface being studied. As the probability of no impact becomes larger, the critical impact speed decreases, this is due to the dependence of the velocity distributions on the dust particle size; as the critical dust particle size increases with the probability of no impact, the critical impact speed decreases.

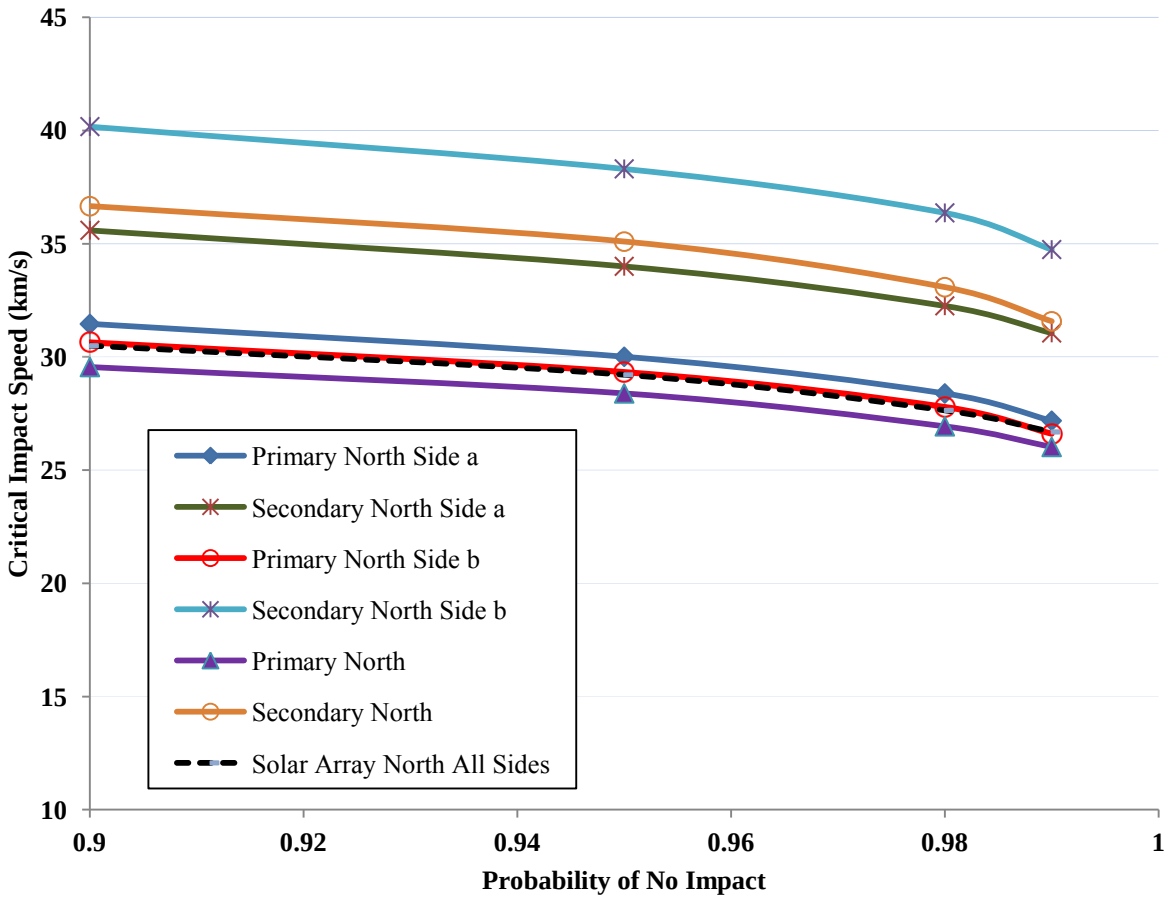

Figure 4.9. - Critical Impact Speed as function of Probability of No Impact

The simulations conducted for the study presented in this thesis produce a large number of plots and numerical results. However in this chapter only a limited number of numerical results are presented in the interest of brevity. For this reason, typical results not included here for collision model "a" using the new methodology, as well as typical results using the old methodology and the no collisions model can be found in Appendix A of this thesis.

CHAPTER 5
RESULTS AND DISCUSSION

5.1 General Introduction

This chapter presents the critical parameters (critical energy, critical particle size and critical impact speed) obtained after performing the integration to determine the cumulative number of impacts and the Monte Carlo simulations for the surfaces of three sections of the spacecraft: the Solar Array North, the Thermal Protection System, and the ISIS Instruments. The results include the three cases discussed in chapter 4: the calculation of critical parameters using the previous methodology considering collision effects; the calculation of critical parameters using the new methodology considering collision effects; and the calculation of critical parameters using the new methodology not considering collision effects.

5.2 Solar Array North Results

Figure 4.4 showed the geometry of Solar Array North, and the total number of impacts of a particle of size 424.3138 μm. Table 5.1 presents the critical energy in Joules, critical dust particle size in μm, and critical impact speed in km/s respectively obtained from the simulations for every surface analyzed in Solar Array North for all three cases discussed earlier. From these results, it can be seen that the critical particle size remains the same regardless of whether the old or the new methodology is used, however the critical particle size increases considerably when collision effects are ignored, this is because models of particle self destruction through collisions are not taken into account. Critical particle sizes for the Primary North side “a” range from 146.19 μm for a PNI of 0.90 to 269.34 μm for a PNI of 0.99 for both the old and new

methodologies. Primary North "b" presents very similar results, both surfaces are almost equally exposed to dust impact, and have the exact same surface area.

Table 5.1.- Critical Parameters for Solar Array North

Surfaces	Critical Energy (J)												Area (m^2)
	Old Methodology				New Methodology				New Methodoloy-No Collision				
	Probability of No Impact				Probability of No Impact				Probability of No Impact				
	0.9	0.95	0.98	0.99	0.9	0.95	0.98	0.99	0.9	0.95	0.98	0.99	
Primary North Side a	11.31	19.72	40.68	70.47	2.02	3.18	5.88	9.45	35.25	67.31	150.33	273.29	0.58
Secondary North Side a	4.70	8.29	16.86	28.97	1.14	1.80	3.26	5.16	11.65	23.11	53.77	98.35	0.17
Primary North Side b	11.05	19.11	39.22	67.23	2.02	3.20	5.94	9.53	28.17	53.84	120.22	216.15	0.58
Secondary North Side b	6.87	11.94	24.30	41.24	1.61	2.50	4.49	6.96	20.52	40.52	92.61	171.63	0.17
Primary North	19.17	33.36	69.38	123.10	3.10	5.00	9.48	15.63	58.76	110.17	244.53	438.30	1.16
Secondary North	10.05	17.42	35.18	60.78	2.15	3.36	6.06	9.54	31.27	60.02	135.24	243.44	0.34
Solar Array North All Sides	25.12	43.75	91.35	161.43	4.14	6.67	12.63	20.81	84.03	156.82	343.75	613.20	1.50

Surfaces	Critical Particle Diameter (um)												Area (m^2)
	Old Methodology				New Methodology				New Methodoloy-No Collision				
	Probability of No Impact				Probability of No Impact				Probability of No Impact				
	0.9	0.95	0.98	0.99	0.9	0.95	0.98	0.99	0.9	0.95	0.98	0.99	
Primary North Side a	146.19	175.43	223.47	269.34	146.19	175.43	223.47	269.34	257.26	316.95	412.29	499.86	0.58
Secondary North Side a	111.24	133.42	168.54	201.40	111.24	133.42	168.54	201.40	183.28	227.86	299.39	365.30	0.17
Primary North Side b	148.67	178.40	227.32	274.01	148.67	178.40	227.32	274.01	252.74	311.52	405.38	491.61	0.58
Secondary North Side b	115.08	137.54	173.13	206.54	115.08	137.54	173.13	206.54	198.91	246.73	323.34	393.85	0.17
Primary North	175.74	211.68	271.33	327.92	175.74	211.68	271.33	327.92	311.86	382.49	495.10	598.41	1.16
Secondary North	134.65	161.01	203.76	244.56	134.65	161.01	203.76	244.56	235.89	291.25	379.75	461.08	0.34
Solar Array North All Sides	189.49	228.61	293.45	354.76	189.49	228.61	293.45	354.76	342.16	418.81	540.94	652.96	1.50

Surfaces	Critical Impact Speed (km/s)												Area (m^2)
	Old Methodology				New Methodology				New Methodoloy-No Collision				
	Probability of No Impact				Probability of No Impact				Probability of No Impact				
	0.9	0.95	0.98	0.99	0.9	0.95	0.98	0.99	0.9	0.95	0.98	0.99	
Primary North Side a	74.39	74.71	74.63	74.23	31.45	30.01	28.39	27.18	56.25	56.83	57.25	57.82	0.58
Secondary North Side a	72.22	73.05	73.35	73.61	35.59	34.00	32.26	31.06	53.76	54.63	55.33	55.52	0.17
Primary North Side b	71.66	71.72	71.42	70.66	30.64	29.33	27.79	26.61	51.63	52.17	52.51	52.72	0.58
Secondary North Side b	82.98	83.73	84.58	84.57	40.17	38.31	36.36	34.74	63.12	64.21	64.70	65.51	0.17
Primary North	73.47	73.31	72.85	73.03	29.55	28.39	26.94	26.02	54.40	54.85	55.49	55.90	1.16
Secondary North	79.32	79.85	79.71	79.68	36.66	35.09	33.08	31.57	60.33	60.92	61.43	61.60	0.34
Solar Array North All Sides	75.11	74.80	74.32	74.32	30.50	29.21	27.64	26.69	56.61	57.11	57.60	58.01	1.50

From Table 5.1 the critical impact speeds can be observed to change dramatically from case to case. For instance the highest critical speeds are observed on Secondary North Side “b” for all three cases. However when using the old methodology the critical impact speeds increase as the PNI increases, ranging from 82.98 km/s for a PNI of 0.90 to 84.57 km/s for a PNI of 0.99; while for the new methodology case the critical impact speeds decrease as the PNI increases, ranging from 40.17 km/s for a PNI of 0.90 to 34.74 km/s for a PNI of 0.99. This is the result of the dependence of the critical impact speed on the dust particle size which proves that the new methodology approach provides less conservative results.

5.3 Thermal Protection System Results

Figure 5.1 shows the geometry of the Thermal Protection System (TPS) and the total number of impacts for a particle of 424.3138 μm.

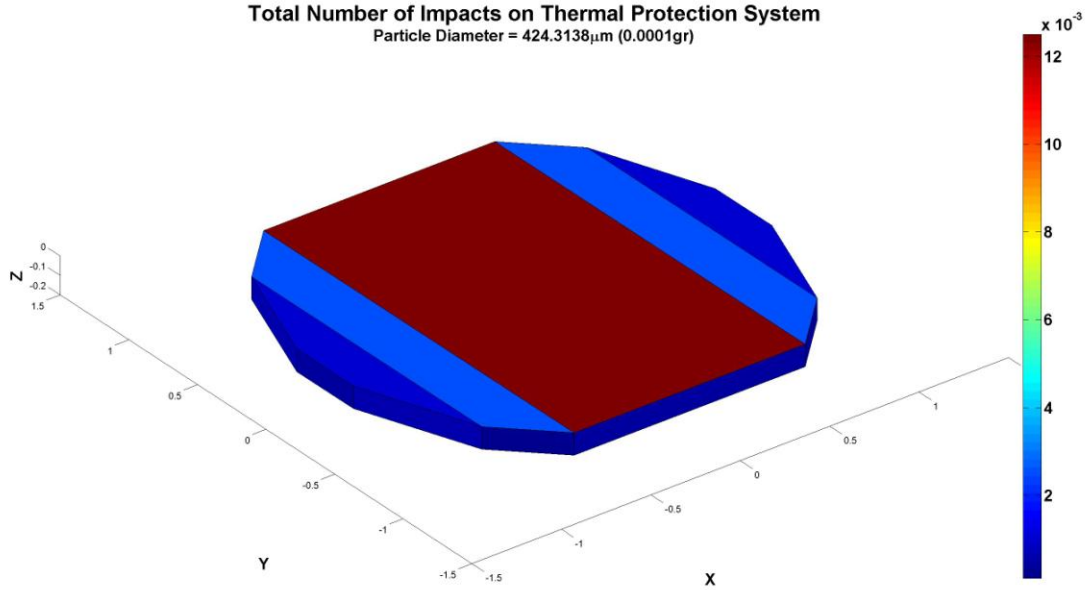

Figure 5.1 Total Number of Impacts on Thermal Protection System

The critical parameters for the TPS are shown in Table 5.2. The TPS will always be facing the sun and the area exposed to particle impacts is relatively large. The critical particle size for the top surface of the TPS ranges from 269.67 μm for a PNI of 0.90 to 507.23 μm for a PNI of 0.99 for both old and new methodologies. If collision effects are ignored, the critical particle size for the top surface of the TPS will be 953.75 μm for a PNI of 0.99. Just as with the Solar Array North the critical impact speed changes considerably from old methodology to new methodology. In the old methodology calculation for the top surface of the TPS the critical impact speed for a PNI of 0.99 is equal to 61.17 km/s, whereas for the new methodology is equal to 27.58 km/s. For the new methodology as the critical particle size increases, the critical impact speed is expected to decrease; this is because of the cumulative density surfaces as function of particle size and normal impact speed described in chapter 4, where as the critical particle sizes become larger, the distribution of critical impact speeds concentrates more toward smaller impact speeds. When collision effects are ignored, the cumulative densities as function of normal impact velocities are very similar for every particle size, therefore the critical impact speed remains relatively without major changes as PNI and critical particle sizes increase. For instance, the TPS top surface critical speed ignoring collision for PNI values from 0.90 to 0.99 remains within 46 km/s

Table 5.2.- Critical Parameters for Thermal Protection System

Surfaces	Critical Energy (J)												Area (m^2)
	Old Methodology				New Methodology				New Methodoloy-No Collision				
	Probability of No Impact				Probability of No Impact				Probability of No Impact				
	0.9	0.95	0.98	0.99	0.9	0.95	0.98	0.99	0.9	0.95	0.98	0.99	
TPS Top Surface	50.23	87.26	183.55	319.63	11.94	19.73	38.34	64.95	184.84	332.51	699.90	1218.11	4.55
TPS Edge	53.13	94.14	198.33	346.52	6.27	9.49	17.15	27.57	158.35	302.53	679.07	1220.42	0.89
TPS Leading Edge	23.41	40.79	82.49	140.85	5.78	8.47	14.81	23.45	142.24	270.94	611.88	1119.31	0.30
TPS Trailing Edge	1.23	2.25	4.88	8.72	0.88	1.56	3.31	5.84	2.60	4.96	11.07	20.00	0.30
TPS Bottom Surface	81.72	141.80	299.98	530.77	12.59	19.82	36.56	58.18	479.64	874.59	1859.83	3268.63	4.55
TPS All	133.79	235.63	498.52	871.74	21.55	35.45	68.59	114.56	705.84	1274.03	2694.86	4705.75	10.00

Surfaces	Critical Particle Diameter (um)												Area (m^2)
	Old Methodology				New Methodology				New Methodoloy-No Collision				
	Probability of No Impact				Probability of No Impact				Probability of No Impact				
	0.9	0.95	0.98	0.99	0.9	0.95	0.98	0.99	0.9	0.95	0.98	0.99	
TPS Top Surface	269.67	326.82	420.21	507.23	269.67	326.82	420.21	507.23	509.50	619.13	793.62	953.73	4.55
TPS Edge	176.20	213.27	274.67	332.78	176.20	213.27	274.67	332.78	304.46	373.63	483.93	585.13	0.89
TPS Leading Edge	118.62	142.03	179.46	214.80	118.62	142.03	179.46	214.80	238.15	293.97	383.26	465.33	0.30
TPS Trailing Edge	150.02	182.14	234.89	284.80	150.02	182.14	234.89	284.80	210.80	261.13	341.55	415.46	0.30
TPS Bottom Surface	229.76	277.17	355.22	428.56	229.76	277.17	355.22	428.56	474.96	577.80	741.49	891.65	4.55
TPS All	312.89	379.89	488.54	589.42	312.89	379.89	488.54	589.42	609.07	738.26	943.95	1132.79	10.00

Surfaces	Critical Impact Speed (km/s)												Area (m^2)
	Old Methodology				New Methodology				New Methodoloy-No Collision				
	Probability of No Impact				Probability of No Impact				Probability of No Impact				
	0.9	0.95	0.98	0.99	0.9	0.95	0.98	0.99	0.9	0.95	0.98	0.99	
TPS Top Surface	62.56	61.80	61.48	61.17	30.50	29.39	28.10	27.58	46.21	46.27	46.25	46.32	4.55
TPS Edge	121.81	121.77	120.93	119.86	41.86	38.66	35.56	33.81	92.59	94.14	95.68	96.48	0.89
TPS Leading Edge	146.40	147.48	147.67	147.36	72.76	67.20	62.56	60.12	126.84	127.65	128.87	130.28	0.30
TPS Trailing Edge	23.57	23.85	23.98	24.01	19.93	19.85	19.76	19.66	20.58	20.63	20.60	20.64	0.30
TPS Bottom Surface	101.46	100.87	101.12	101.50	39.83	37.71	35.30	33.61	82.70	83.23	83.49	83.93	4.55
TPS All	81.69	81.04	80.82	80.65	32.79	31.43	29.98	29.24	69.09	69.55	69.97	70.33	10.00

5.4 ISIS Instruments Results

The ISIS Instruments are two instruments that will survey elements in the atmosphere of the Sun using a mass spectrometer to sort ions within the whereabouts of Solar Probe Plus. The instruments were divided into several surfaces in order to perform the numerical integration of

impacts, thus several hours of computation were required to complete the integration. The geometry of ISIS and the total number of impacts for a particle size of 424.3138 μm is shown in Figure 5.2.

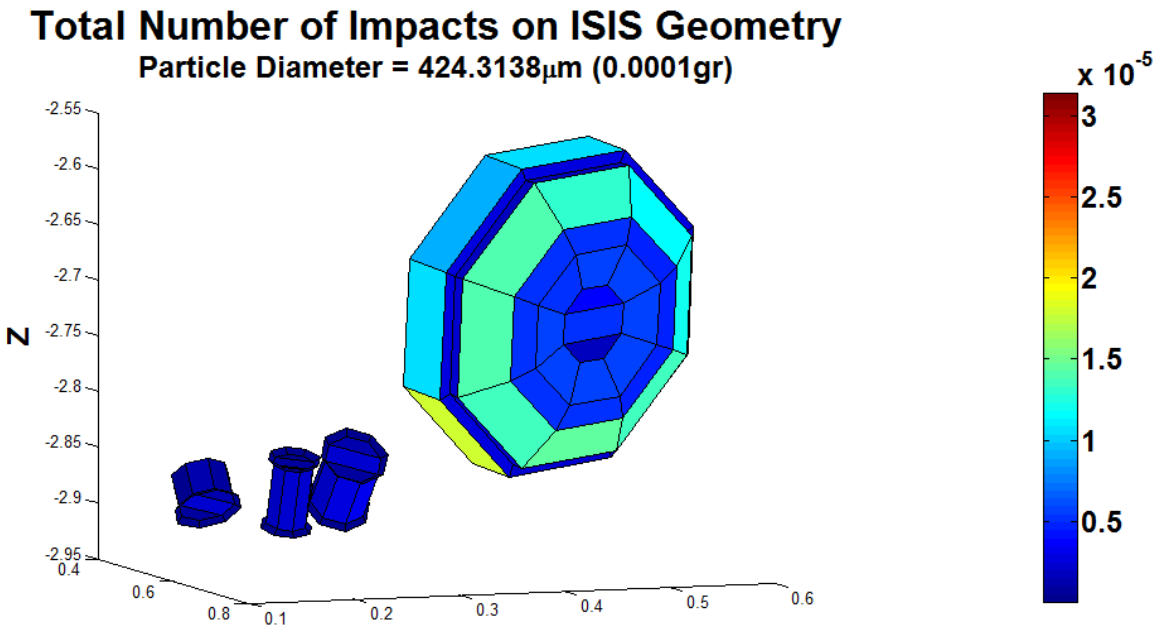

Figure 5.2 Total Number of Impacts on ISIS Geometry

The critical parameters for the ISIS instruments are shown in Table 5.3. The critical parameters for the ISIS instruments were obtained for ten different surfaces, and their areas are far smaller when compared to other Solar Probe Plus components such as the Thermal Protection System. The EPI Low Sensor Surface represents the largest area of the ISIS Instruments surfaces with an area of 0.00753 m². The critical particle sizes obtained for this surface range from 86.59 μm for a PNI of 0.90 to 155.97 μm for a PNI of 0.99 (both previous and new methodology). These critical particle sizes are smaller than those calculated for other components such as the Solar Array North and the Thermal Protection System not only because of their small area but

also because the instruments are often shadowed and protected by other components of the spacecraft during the trajectory of the mission. In the previous methodology the critical impact speeds increase as PNI and particle size increase. Using the new methodology the critical impact speed decreases as the PNI and critical particle size increase, once again this is due to the cumulative density distributions as functions of particle size and normal impact speed. The critical impact speeds for EPI Low Sensor for the new methodology range from 81.51 km/s for a PNI of 0.90 to 63.41 km/s for a PNI of 0.99. In General the critical impact speeds for the ISIS instruments are larger than those seen in the previously discussed components of Solar Probe Plus, and this is because the critical particle sizes are smaller, and their velocity distributions, according to the new methodology are wider and include a greater range of normal impact velocities.

Table 5.3.- Critical Parameters for ISIS Instruments

Surfaces	Critical Energy (J)												Area (m^2)
	Old Methodology				New Methodology				New Methodoloy-No Collision				
	Probability of No Impact				Probability of No Impact				Probability of No Impact				
	0.9	0.95	0.98	0.99	0.9	0.95	0.98	0.99	0.9	0.95	0.98	0.99	
EPI Low Base	3.67	6.54	13.66	23.47	1.20	1.86	3.19	4.65	9.86	20.92	52.56	100.03	0.0583
EPI Low Sensor	7.92	13.92	28.42	47.74	2.82	4.09	6.66	9.98	37.74	76.09	180.32	333.64	0.0753
EPI Hi LET1 Body	0.10	0.26	0.67	1.18	0.06	0.15	0.35	0.61	0.04	0.19	0.85	2.15	0.0012
EPI Hi LET1 Ap1	0.14	0.30	0.72	1.32	0.07	0.13	0.26	0.44	0.10	0.30	0.98	2.18	0.0020
EPI Hi LET1 Ap2	0.23	0.46	0.95	1.57	0.14	0.27	0.54	0.85	0.20	0.60	2.02	4.74	0.0020
EPI Hi HET Body	0.05	0.13	0.38	0.72	0.03	0.08	0.21	0.38	0.02	0.08	0.39	1.06	0.0009
EPI Hi HET Ap1	0.11	0.25	0.59	1.06	0.06	0.12	0.26	0.42	0.08	0.24	0.85	2.00	0.0010
EPI Hi HET Ap2	0.03	0.07	0.18	0.32	0.02	0.05	0.12	0.21	0.01	0.06	0.27	0.66	0.0010
EPI Hi LET2 Body	0.31	0.61	1.36	2.43	0.13	0.23	0.48	0.77	0.24	0.67	2.14	4.83	0.0052
EPI Hi LET2 Ap1	0.35	0.65	1.30	2.15	0.19	0.35	0.66	1.02	0.37	1.02	3.30	7.40	0.0020

Surfaces	Critical Particle Diameter (um)												Area (m^2)
	Old Methodology				New Methodology				New Methodoloy-No Collision				
	Probability of No Impact				Probability of No Impact				Probability of No Impact				
	0.9	0.95	0.98	0.99	0.9	0.95	0.98	0.99	0.9	0.95	0.98	0.99	
EPI Low Base	79.53	96.33	122.20	145.49	79.53	96.33	122.20	145.49	132.90	167.41	222.42	273.31	0.0583
EPI Low Sensor	86.59	104.17	131.33	155.97	86.59	104.17	131.33	155.97	164.14	204.72	269.93	330.15	0.0753
EPI Hi LET1 Body	23.36	30.41	38.70	45.60	23.36	30.41	38.70	45.60	21.28	32.88	50.44	67.70	0.0012
EPI Hi LET1 Ap1	35.40	43.99	57.57	70.01	35.40	43.99	57.57	70.01	38.15	53.08	77.74	100.73	0.0020
EPI Hi LET1 Ap2	31.18	37.48	46.53	55.48	31.18	37.48	46.53	55.48	34.51	47.97	71.03	93.05	0.0020
EPI Hi HET Body	19.49	26.84	35.40	41.70	19.49	26.84	35.40	41.70	15.84	26.78	42.81	58.02	0.0009
EPI Hi HET Ap1	29.99	37.56	48.65	59.03	29.99	37.56	48.65	59.03	30.39	43.40	65.01	85.50	0.0010
EPI Hi HET Ap2	21.94	29.17	37.64	44.37	21.94	29.17	37.64	44.37	19.09	30.43	47.36	63.82	0.0010
EPI Hi LET2 Body	38.14	46.25	59.79	72.58	38.14	46.25	59.79	72.58	45.00	61.44	88.85	114.20	0.0052
EPI Hi LET2 Ap1	35.18	41.59	52.00	62.05	35.18	41.59	52.00	62.05	42.67	58.46	84.97	109.62	0.0020

Surfaces	Critical Impact Speed (km/s)												Area (m^2)
	Old Methodology				New Methodology				New Methodoloy-No Collision				
	Probability of No Impact				Probability of No Impact				Probability of No Impact				
	0.9	0.95	0.98	0.99	0.9	0.95	0.98	0.99	0.9	0.95	0.98	0.99	
EPI Low Base	105.64	105.69	106.95	107.92	60.47	56.41	51.71	48.04	80.12	82.54	85.43	86.52	0.0583
EPI Low Sensor	136.51	137.19	138.46	138.65	81.51	74.36	67.05	63.41	114.19	116.41	118.36	119.02	0.0753
EPI Hi LET1 Body	110.21	119.32	133.09	137.63	88.02	90.33	96.63	99.52	84.33	91.28	100.55	102.81	0.0012
EPI Hi LET1 Ap1	69.42	73.49	76.06	76.55	49.14	48.17	46.03	44.02	53.36	55.17	56.43	57.12	0.0020
EPI Hi LET1 Ap2	107.36	115.34	119.88	118.59	84.67	88.69	90.72	87.29	85.30	91.20	92.87	94.86	0.0020
EPI Hi HET Body	97.23	101.30	114.20	123.14	81.32	80.15	85.96	89.21	78.70	77.90	87.05	91.23	0.0009
EPI Hi HET Ap1	80.38	84.80	88.15	88.82	59.79	59.59	58.47	56.05	64.24	67.24	68.90	69.99	0.0010
EPI Hi HET Ap2	64.81	67.58	72.45	75.21	56.25	57.00	59.58	60.76	55.83	57.90	61.78	62.06	0.0010
EPI Hi LET2 Body	91.87	97.39	98.71	98.62	59.05	60.19	58.70	55.65	63.35	66.32	68.34	70.40	0.0052
EPI Hi LET2 Ap1	110.45	117.20	118.69	117.16	81.99	85.71	84.92	80.81	85.60	88.44	90.63	92.63	0.0020

CHAPTER 6

SUMMARY, CONCLUSION AND RECOMMENDATIONS

6.1 Summary

To understand how the critical parameters for the design of protective equipment for the Solar Probe Plus spacecraft are obtained, this thesis presented the studies that have been conducted throughout to understand how dust particle environments behave and how to model them as accurate as possible. Several research articles and reports that attempted to model these dust environments were described. Background on dust protection techniques was also introduced by describing reports and concerning this topic.

This thesis described in detail a particular model presented in Mann *et al* 2004, and the equations that determine the flux of dust particles for certain assumed conditions. This model was used in the numerical integration to find the critical parameters for Solar Probe Plus. A description of the methods that NASA uses to asses risk of micrometeoroid and orbital debris impact was presented, different shielding concepts were discussed as well as examples of typical shielding configurations for which NASA had developed ballistic limit equations to evaluate performance.

A description of the Solar Probe Plus mission, and the geometry of the spacecraft was presented. The previous methodology and the methodology proposed in this thesis that are used for the determination of critical parameters for Solar Probe Plus were explained. The discussion of the methodologies included concepts of probability of no impact (PNI), and how the integration to calculate the cumulative number of impacts on a particular surface of the spacecraft was performed. This new proposed methodology to select critical parameters was

compared to the previously developed methodology. The previous methodology used the cumulative number of impacts as a function of particle mass and a cumulative density function of number of impacts as a function of normal impact speeds for the smallest particle mass to perform Monte Carlo simulations. The new methodology used a cumulative density function of number of impacts as a function of both particle size and normal impact velocity; this approach resulted in less conservative results since the critical impact speed depended on the dust particle size; for instance smaller particle sizes had wider normal speed distributions resulting in higher critical impact speeds; and larger particle sizes had narrower particle distributions resulting in smaller critical impact speeds.

Results of critical parameters such as critical energy, critical particle size, and critical impact speed were presented for three different components of Solar Probe Plus: the Solar Array North, the Thermal Protection System, and the Isis Instruments. The critical parameters for all three components were obtained for three different cases, the previous methodology, the new methodology and ignoring particle collision effects. The new methodology proved to reduce the conservatism of the previous methodology.

6.2 Conclusion

Current Probability of No Impact concepts are widely accepted to address critical particle size for low earth orbit missions, however when the distribution of impact speeds as function of particle varies significantly because of spacecraft trajectories, the calculation of critical impact speeds becomes more difficult to perform. The results presented in this thesis show that a new methodology which considers the cumulative number of impacts as a function of particle size and normal impact velocities produces less conservative results than previous attempts which

considered only the distribution of the smallest particle (which had the wider distribution of speeds). The new methodology considers relationship between the critical particle size and its corresponding normal impact speed distribution. The bigger critical particle sizes show a narrower distribution of speeds concentrated towards smaller impact speeds, while the smaller particle sizes have a wider range of impact speeds that can reach high values. The determination of critical impact speed is crucial since the level of damage to a component of the spacecraft is proportional to the kinetic energy released during the event of an impact. The new methodology presents an approach on calculating critical parameters that can significantly reduce conservatism in the design of dust impact protection, and therefore the levels protection and mass, which will also reduce the cost of materials and launch of Solar Probe Plus.

6.3 Recommendations

To further study the results obtained with the new methodology, sensitivity and reliability analysis are recommended. This can be achieved by performing a reliability study using ballistic limit equations for certain shield configurations using the critical parameters calculated with the new methodology. The reliability study would comprise the calculation of a reliability index on critical particle ballistic limit equations using limit state functions and statistical data for normal impact velocities, impact angles and densities. Several studies would have to be performed for different configurations of shields, and different design conditions; for instance adding variability to normal impact speeds as the critical particle changes size, or even studying how is the critical particle size affected when there is variability introduced in material properties or shield geometries.

REFERENCES

Carrasco C, et al. Preliminary dust-impact risk study for the „„Solar Probe'' spacecraft. International Journal of Impact Engineering 2006;33:133–142

Christiansen E, et al. Ballistic limit equations for spacecraft shielding. International Journal of Impact Engineering 2001;26:93-104

Christiansen E, et al. Enhanced meteoroid and orbital debris shielding. International Journal of Impact Engineering 1995;17:217-228

Christiansen E, et al. Meteoroid and orbital debris risk mitigation in a low earth orbit satellite constellation. International Journal of Impact Engineering 2001;26:345-356

Christiansen E. Meteoroid/debris shielding. NASA Johnson Space Center 2003

Christiansen E, et al. Space station MMOD shielding. Acta Astronautica 2009;65:921-929

Christiansen E. Handbook for designing MMOD Protection, NASA Johnson Space Center 2009

Divine N. Five Populations of Interplanetary Meteoroids. Journal of Geophysical Research 1993;98:17029-17048

Harr M. (1998). Reliability-based design in civil engineering. Dover Publications, INC. Mineola, new York

Ishimoto H, et al. Modeling the particle mass distribution within 1 AU of the Sun. Planetary and Space Science 1999;47:114-121

Jackson A, et al. The capture of interstellar dust: the pure Poynting–Robertson case. Planetary and Space Science 2001;49:417– 424

Johns Hopkins University Applied Physics Laboratory. Solar Probe+ Mission Engineering Study Report, 2008

Johns Hopkins University Applied Physics Laboratory. "Solar Probe Plus: A NASA Mission To Touch The Sun", < http://solarprobe.jhuapl.edu/> November 2011

Kocifaj M, et al. Dynamical behavior of interstellar dust particles in the solar system. Journal of Quantitative Spectroscopy & Radiative Transfer 2004;89:165–177

Kocifaj M, et al. The capture of interstellar dust: the Lorentz force case. Planetary and Space Science 2004;53:839 – 847

Mann I, et al. Dust cloud near the Sun. Icarus 2000;146:568–582

Mann I, et al. Dust measurements at the edge of the solar system. Advances in Space Research 2004,34:179–183

Mann I, et al. Dust near the sun. Space Sci Rev 2004;110:269–305

Ryan S, et al. A ballistic limit analysis programme for shielding against micrometeoroids and orbital debris. Acta Astronautica 2011;69:245-257

Ryan S. et al. Whipple shield performance in the shatter regime. International Journal of Impact Engineering 2011;38:504-510

APPENDIX A: SOLAR ARRAY NORTH

A.1 New Methodology Typical Results

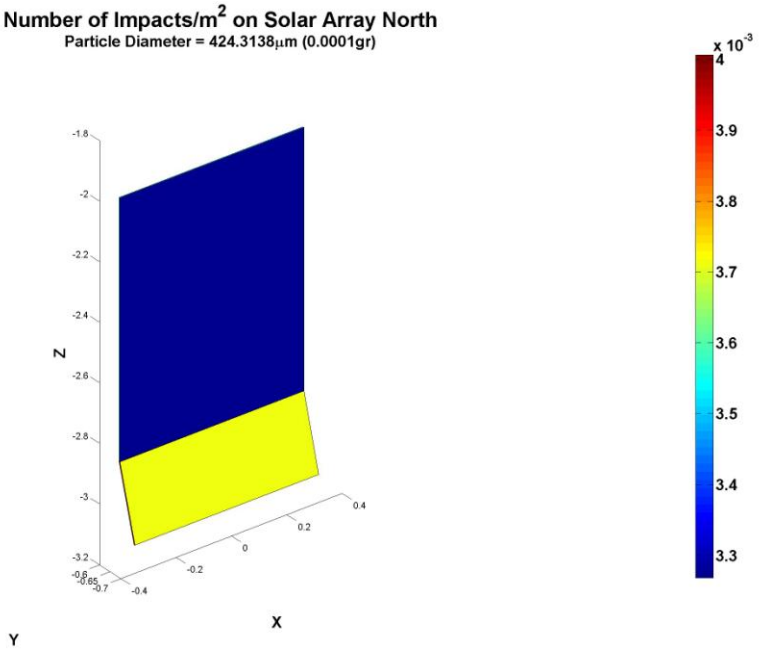

Figure A-1 Number of Impacts/m² on Solar Array North for particle size of 424.31μm (New Methodology)

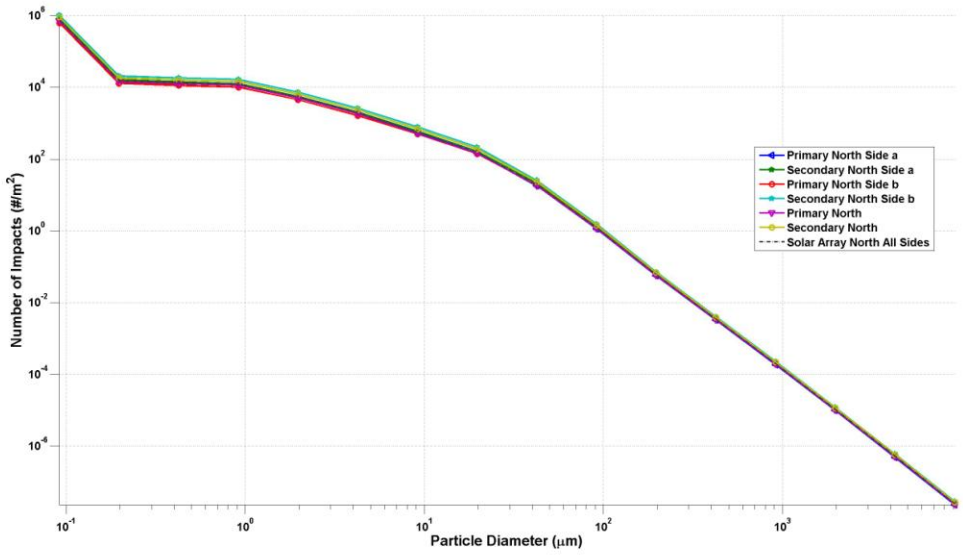

Figure A-2 Number of Impacts/m² on Solar Array North as a function of particle diameter (New Methodology)

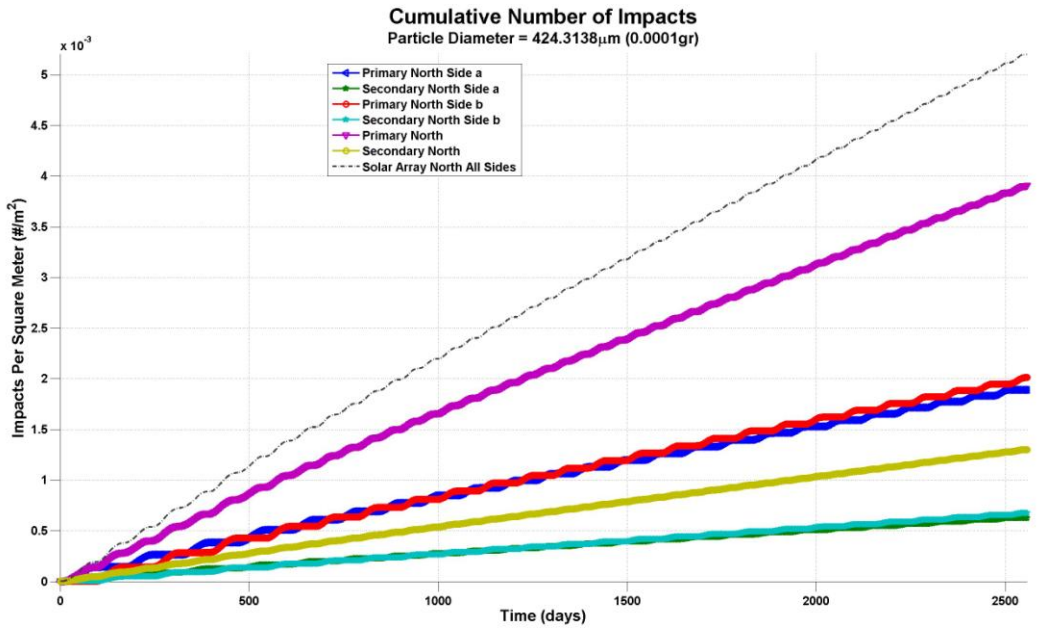

Figure A-3 Cumulative Number of Impacts on Solar Array North as a function of time for particle size of 424.31μm (New Methodology)

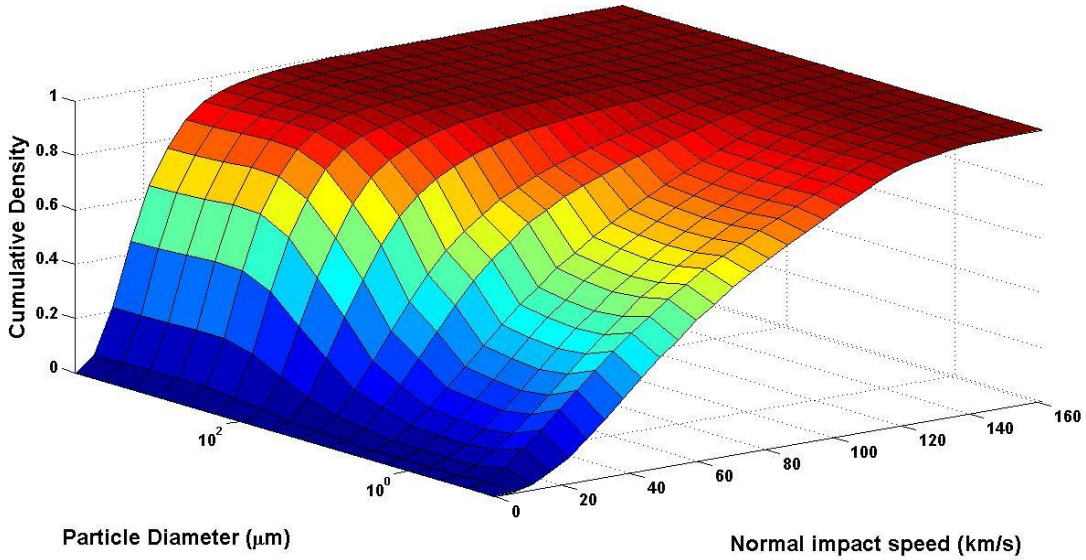

Figure A-4 Cumulative density as function of both particle diameter and normal impact speed for Solar Array North All Sides (New Methodology)

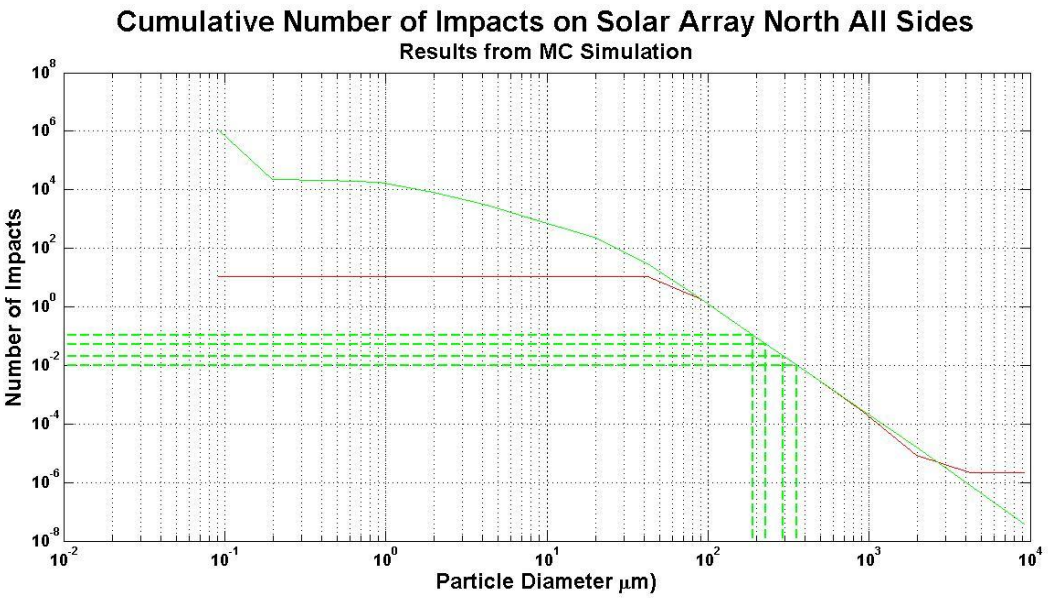

Figure A-5 Cumulative Number of Impacts on Solar Array North All Sides as function of particle diameter (New Methodology)

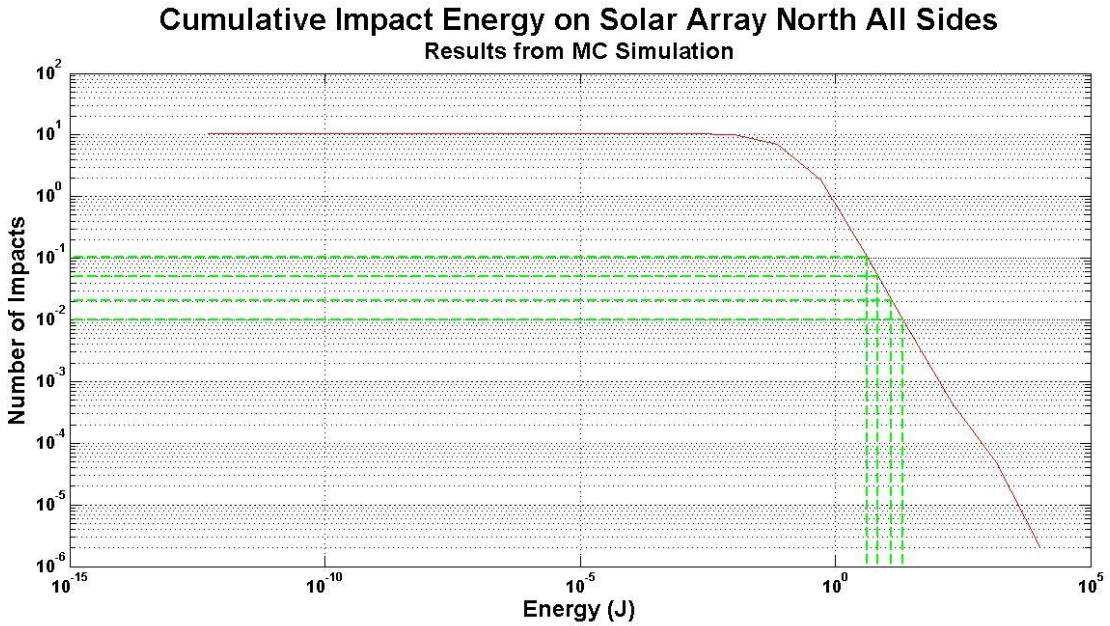

Figure A-6 Cumulative Impact Energy on Solar Array North All Sides (New Methodology)

A.2 Typical Results No Collisions

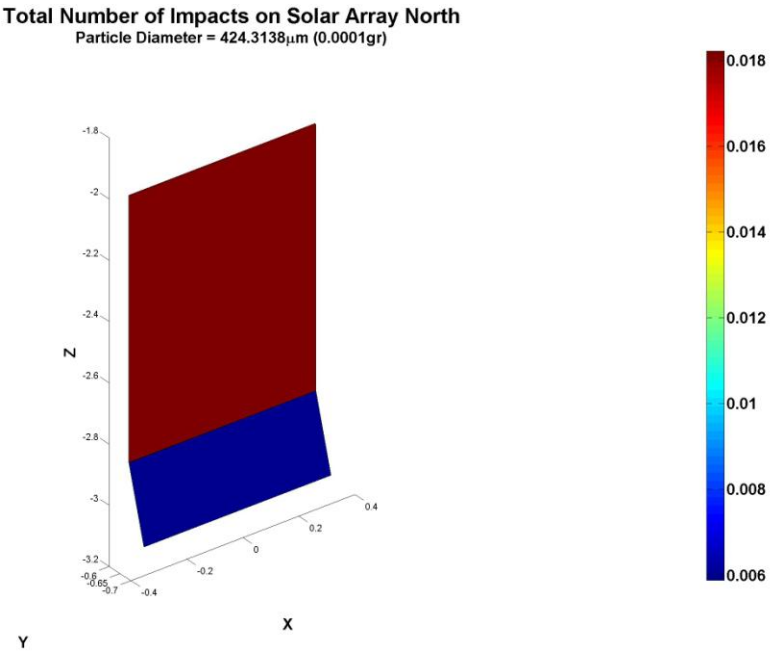

Figure A-7 Number of impacts on Solar Array North for particle size of 424.31μm (No Collisions)

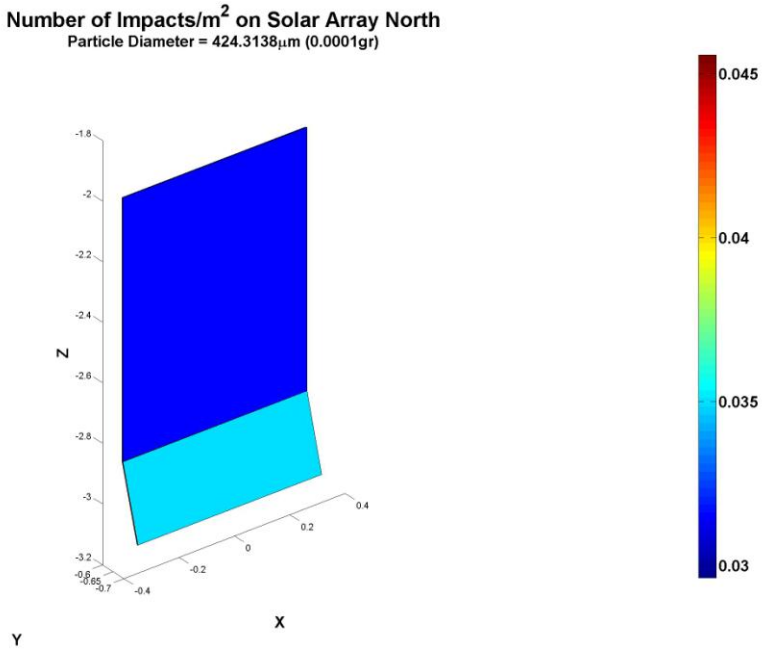

Figure A-8 Number of impacts/m² on Solar Array North for Particle Size of 424.31μm (No Collisions)

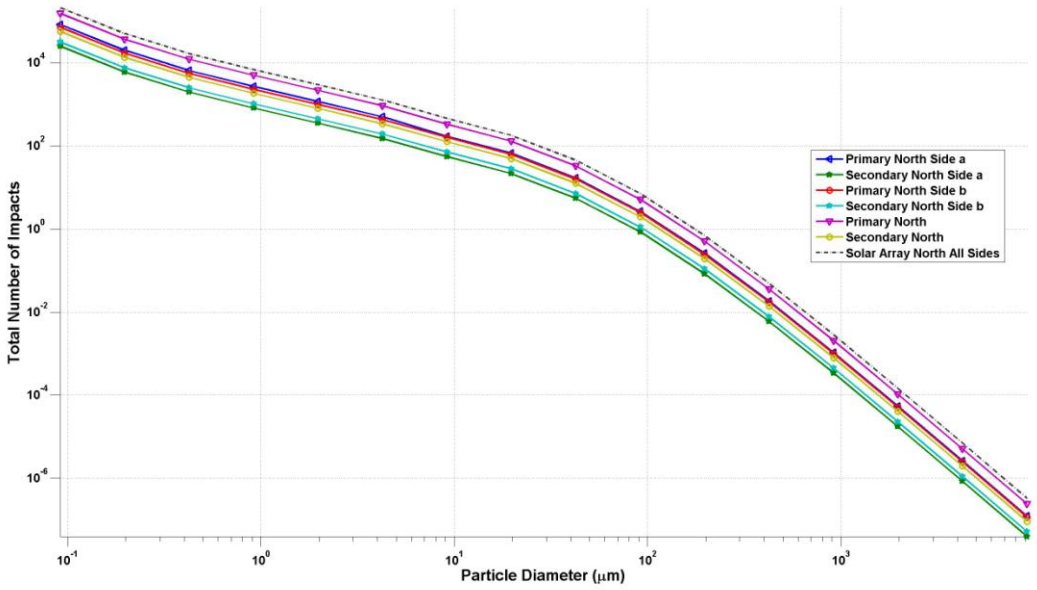

Figure A-9 Number of Impacts on Solar Array North as Function of Particle Size (No Collisions)

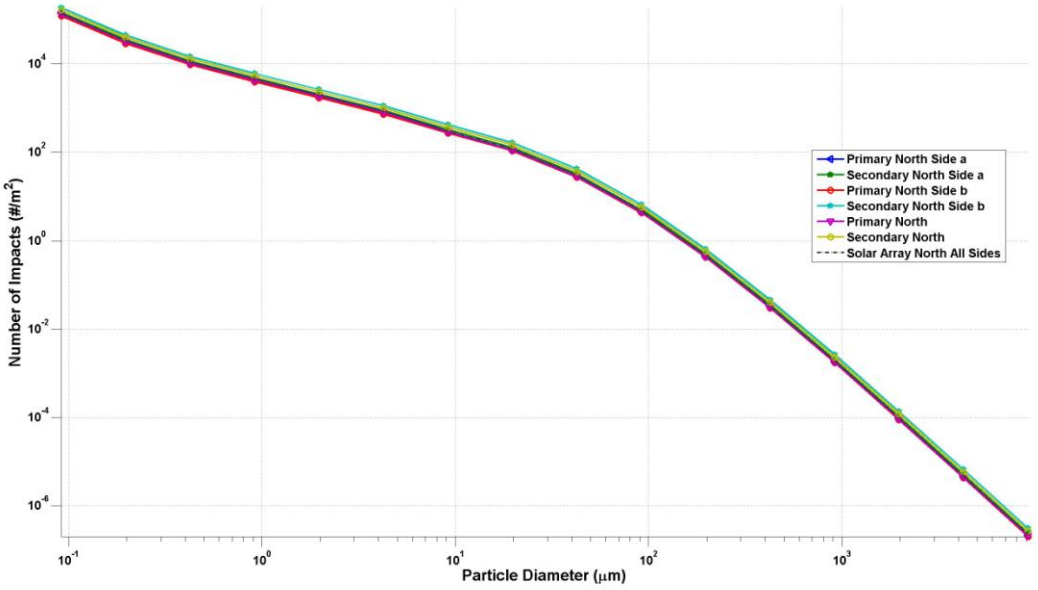

Figure A-10 Number of Impacts/m² on Solar Array North as Function of Particle Size (No Collisions)

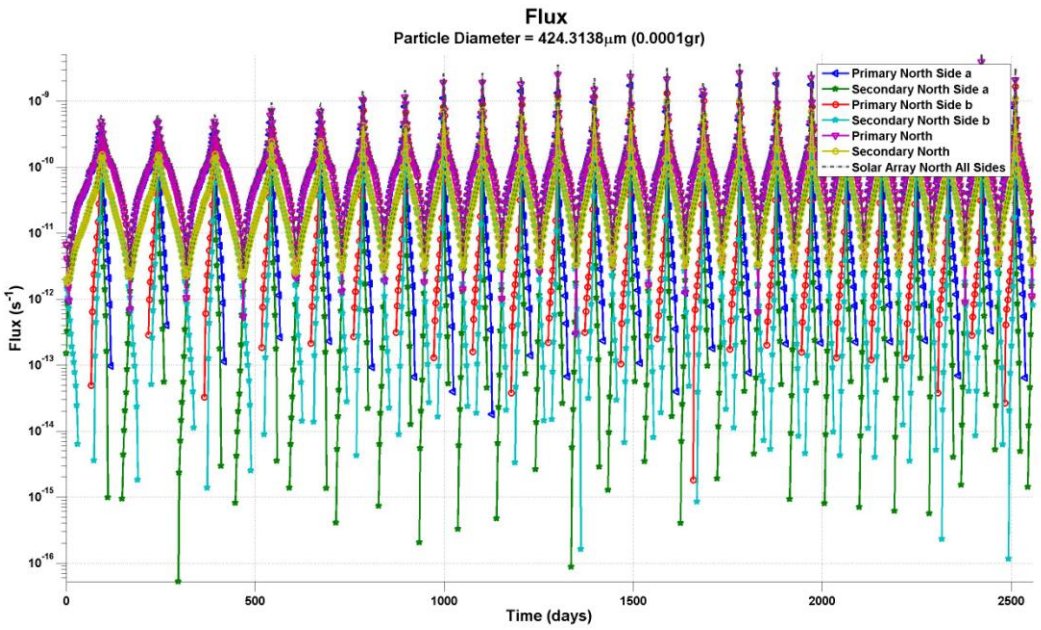

Figure A-11 Flux for Particle of Size 424.31μm on Solar Array North as Function of Time (No Collisions)

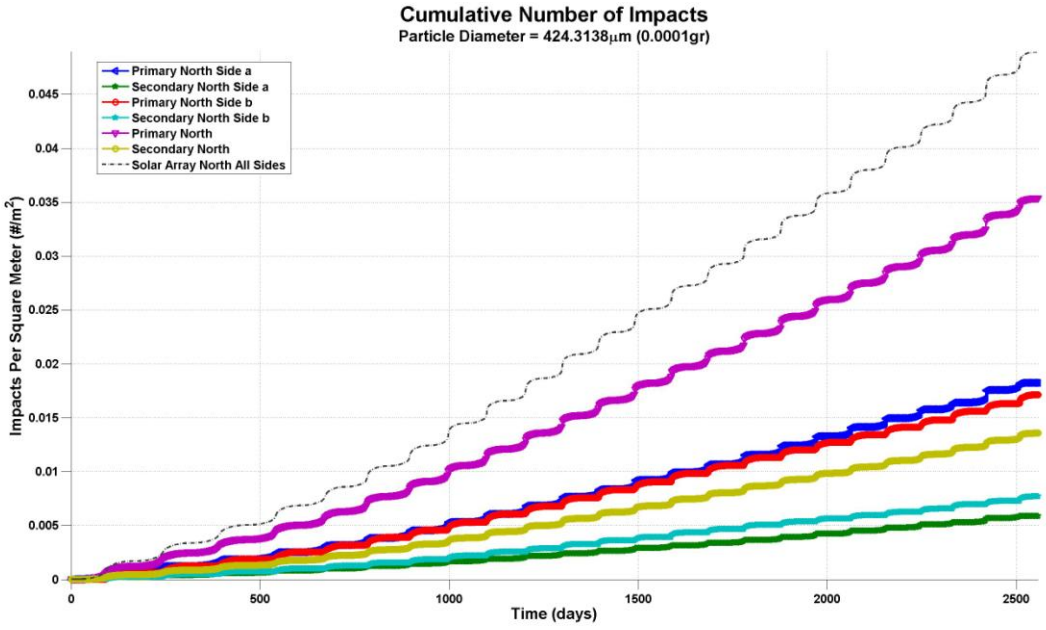

Figure A-12 Cumulative Number of Impacts/m² on Solar Array North as Function of Time (No Collisions)

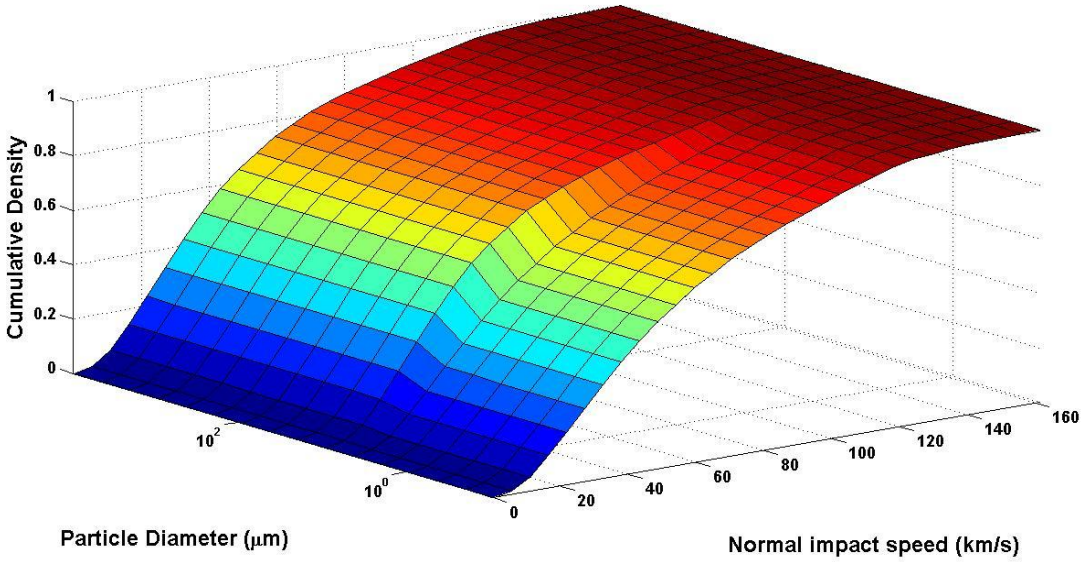

Figure A-13 Cumulative Density as function of both particle diameter and normal impact speed for Solar Array North All Sides (No Collisions)

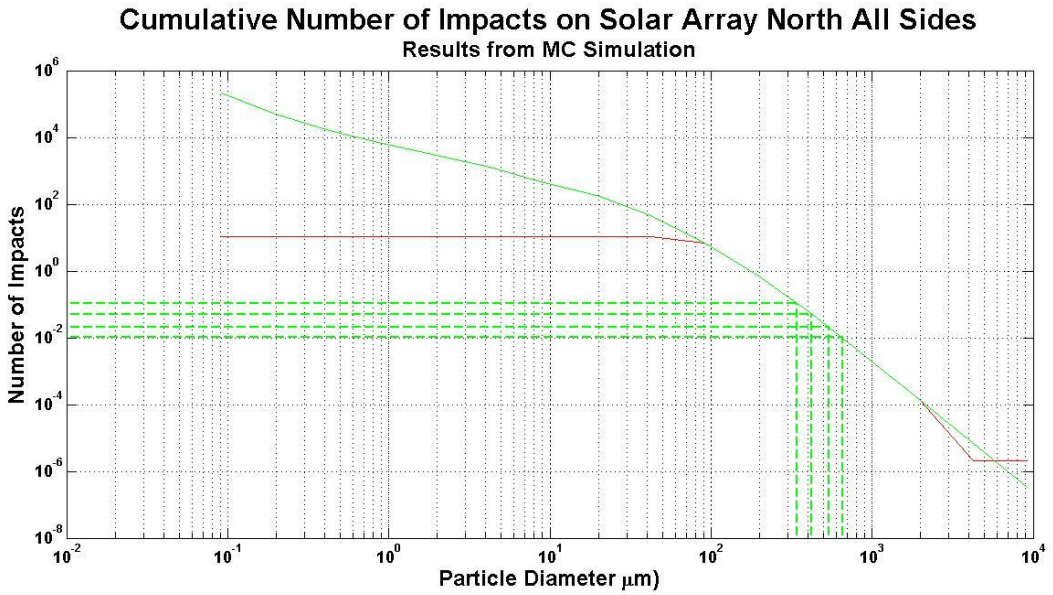

Figure A-14 Cumulative Number of Impacts as function of particle diameter on Solar Array North All Sides (No Collisions)

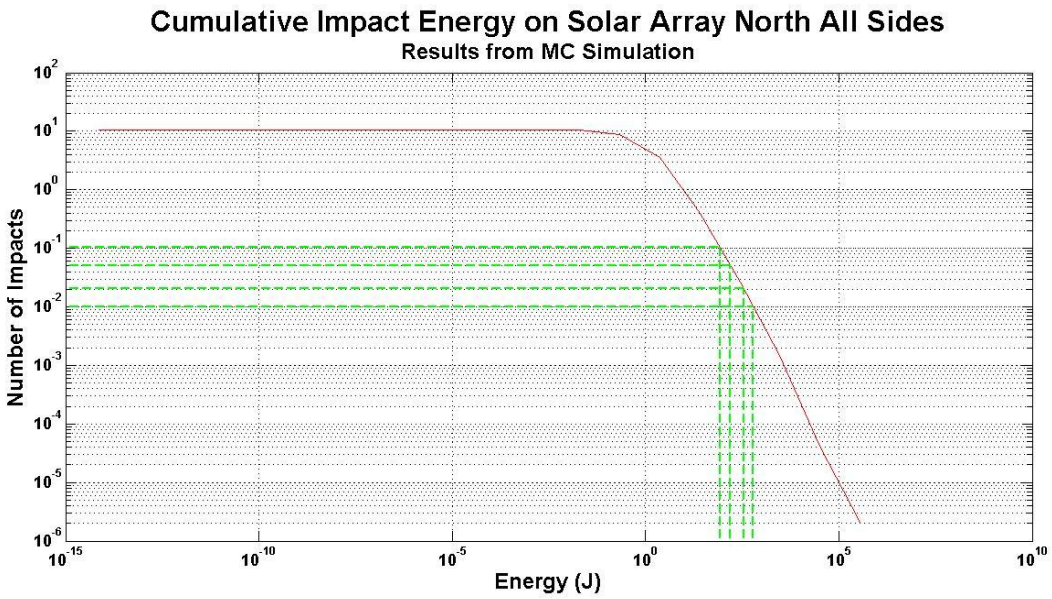

Figure A-15 Cumulative Impact Energy on Solar Array North All Sides (No Collisions)

A.3 Typical Results Old Methodology

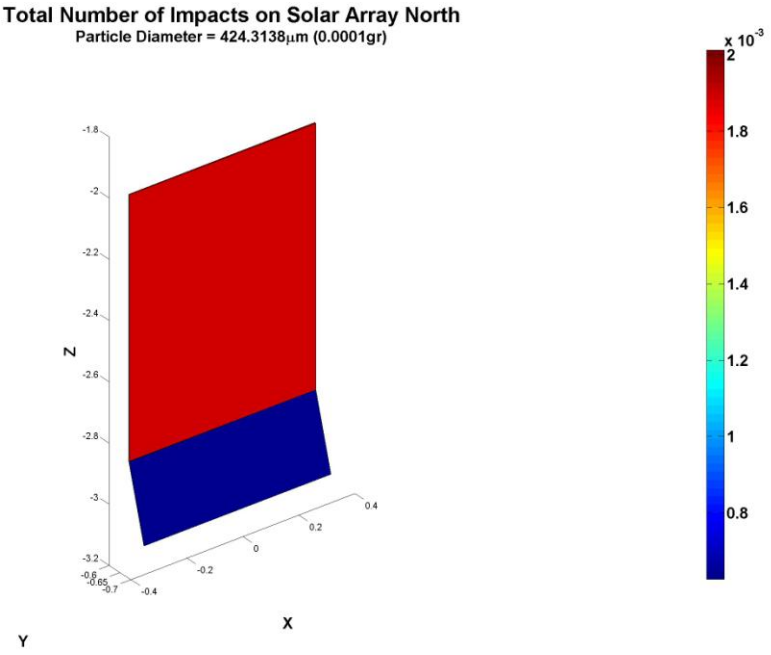

Figure A-16 Number of impacts on Solar Array North for particle size of 424.31μm (Old Methodology)

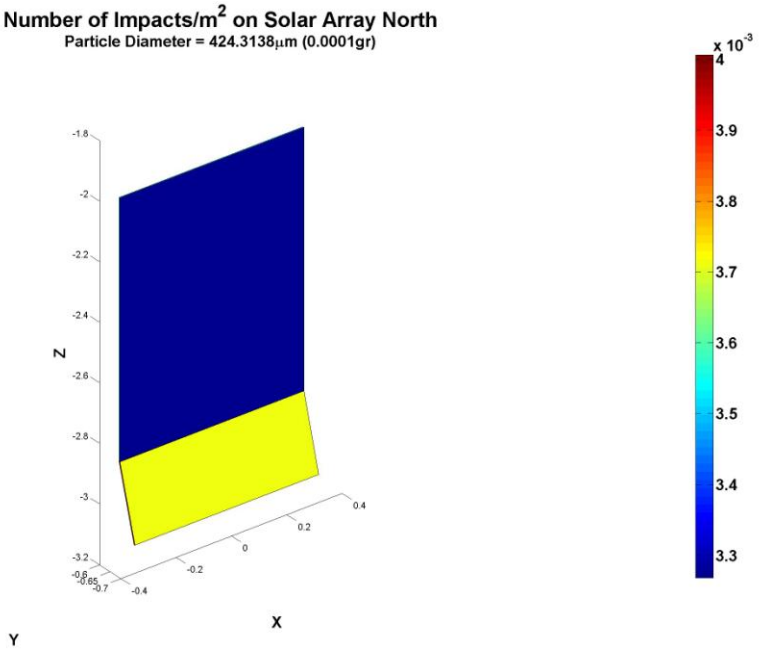

Figure A-17 Number of impacts/m² on Solar Array North for Particle Size of 424.31μm (Old Methodology)

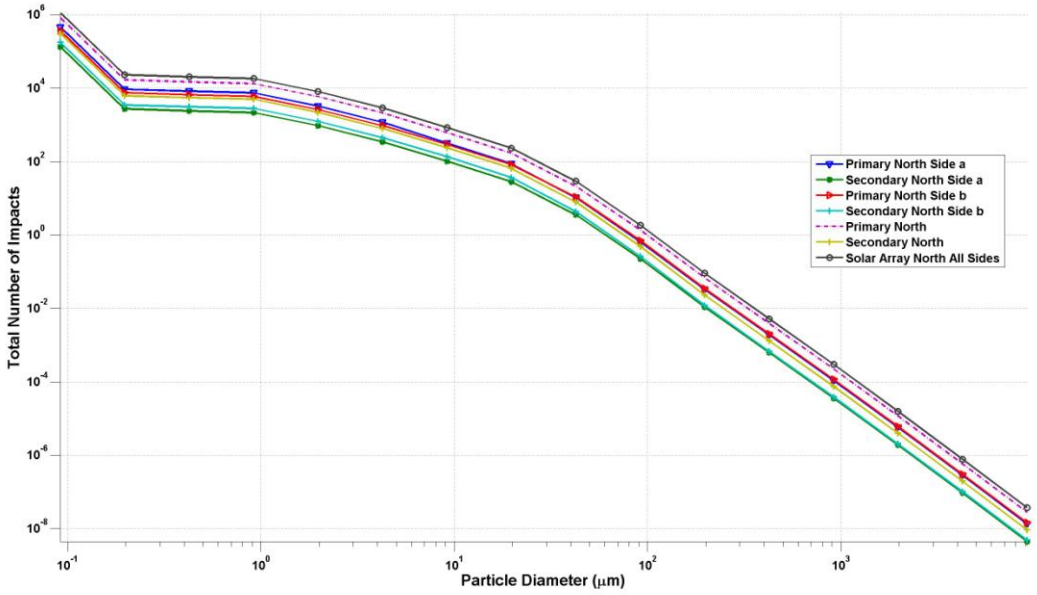

Figure A-18 Number of Impacts on Solar Array North as Function of Particle Size (Old Methodology)

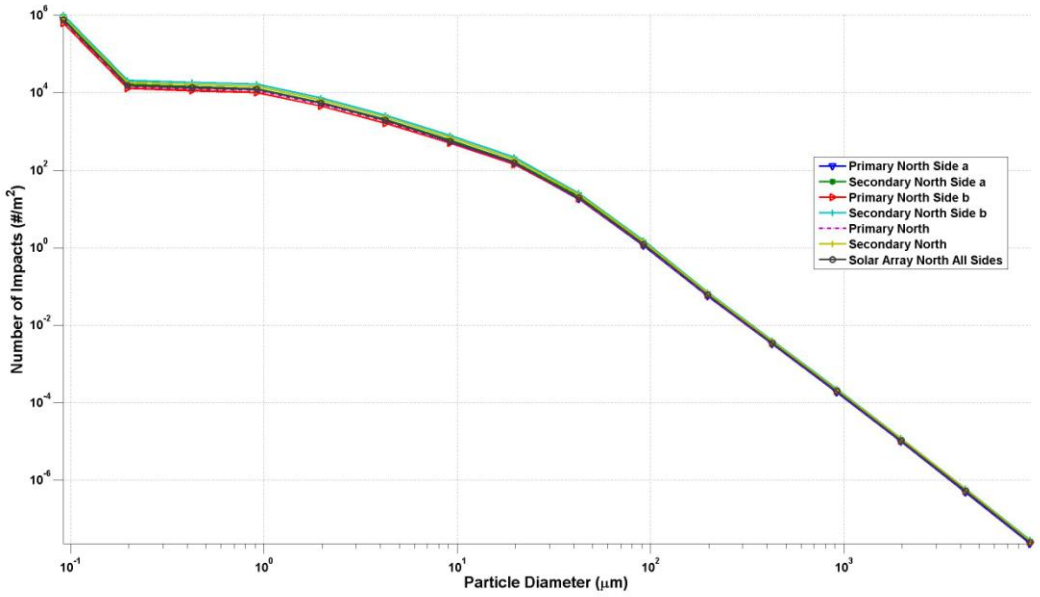

Figure A-19 Number of Impacts/m² on Solar Array North as Function of Particle Size (Old Methodology)

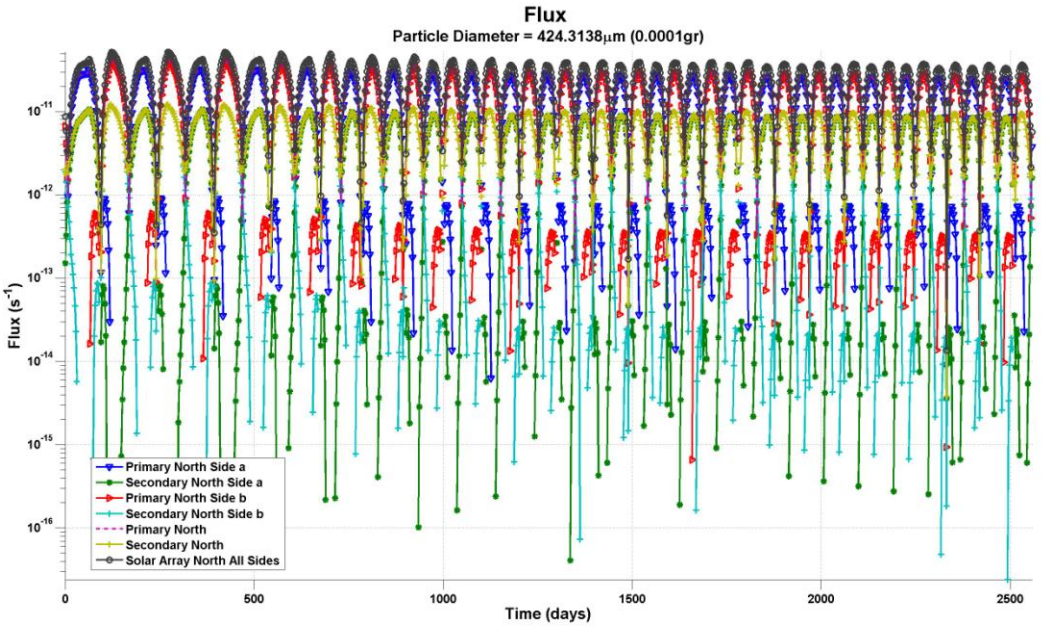

Figure A-20 Flux for Particle of Size 424.31μm on Solar Array North as Function of Time (Old Methodology)

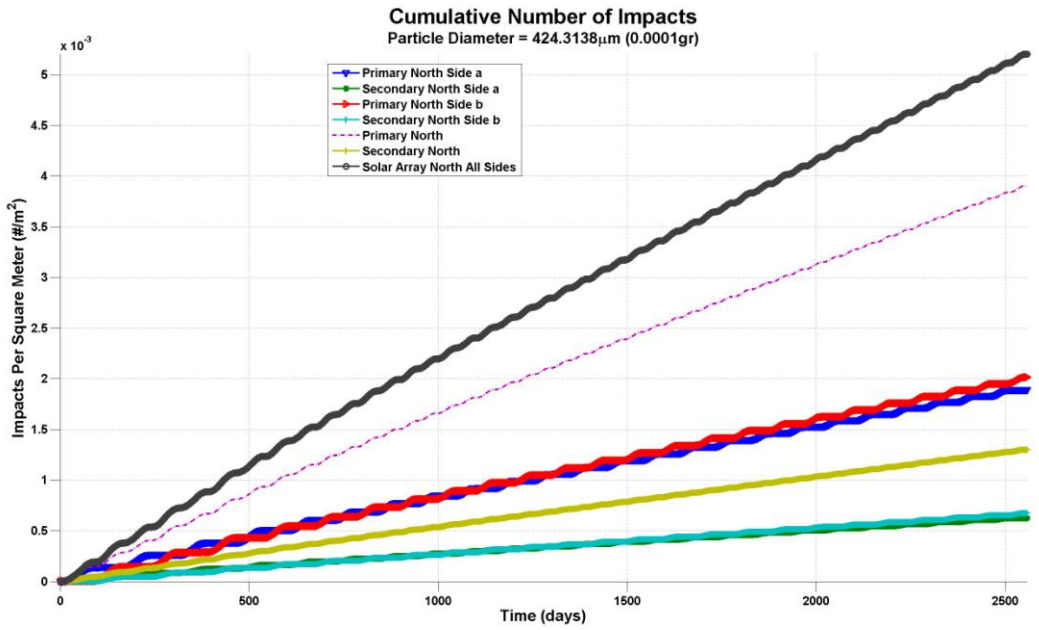

Figure A-21 Cumulative Number of Impacts/m² on Solar Array North as Function of Time (Old Methodology)

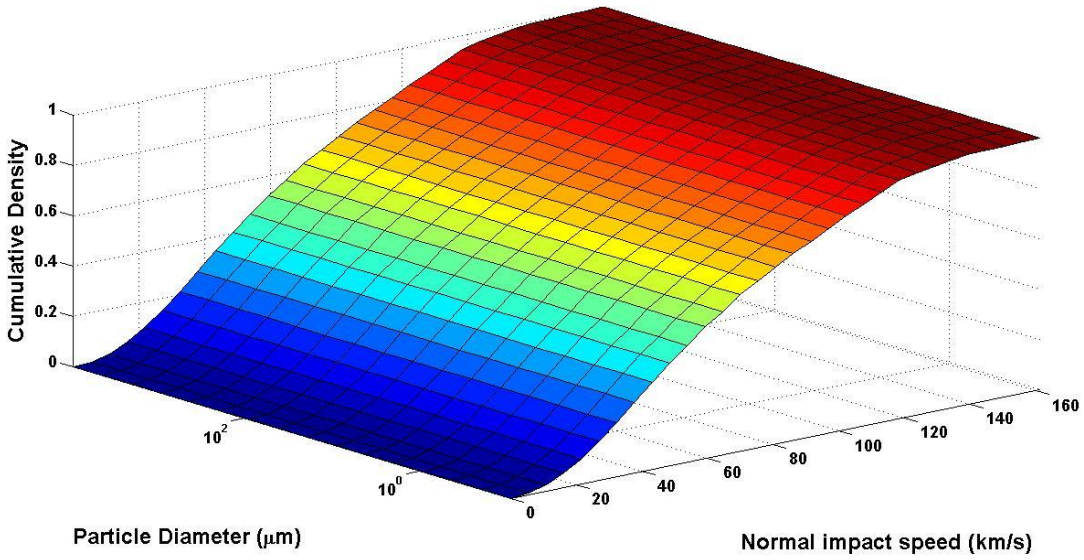

Figure A-22 Cumulative Density as function of both particle diameter and normal impact speed for Solar Array North All Sides (Old Methodology)

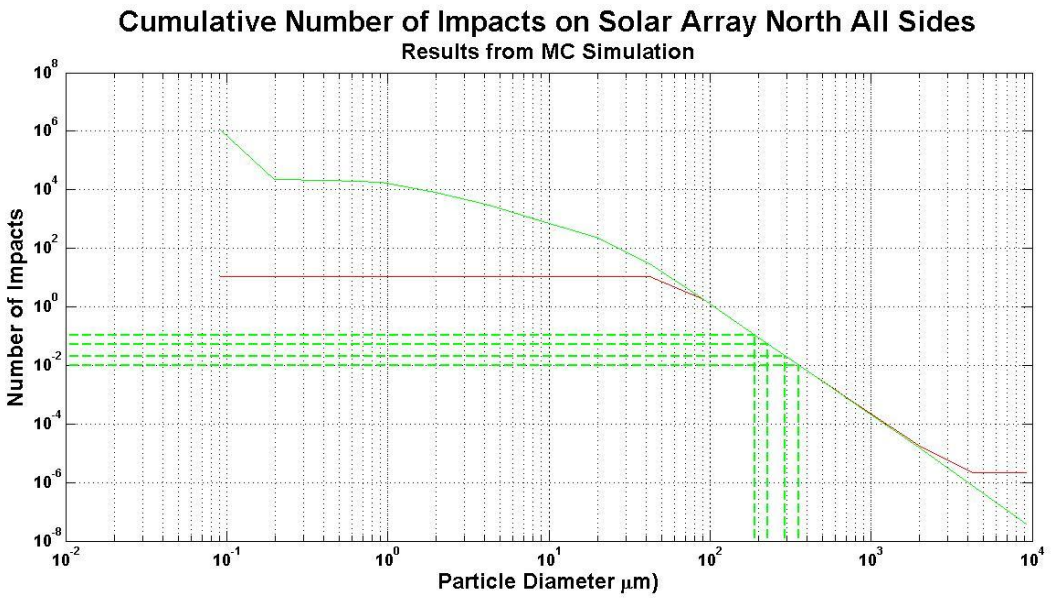

Figure A-23 Cumulative Number of Impacts as function of particle diameter on Solar Array North All Sides (Old Methodology)

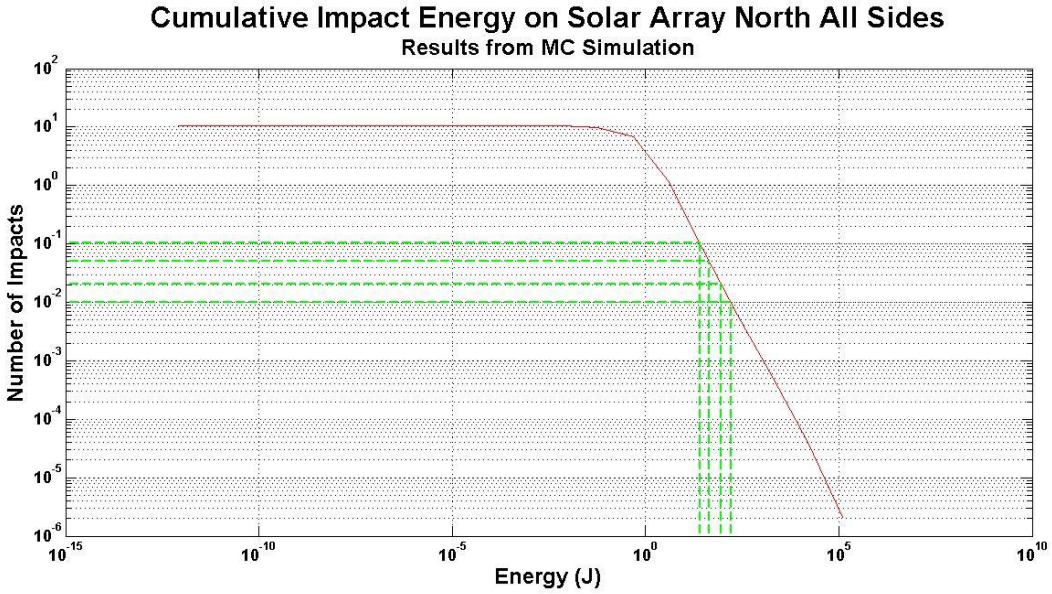

Figure A-24 Cumulative Impact Energy on Solar Array North All Sides (Old Methodology)

CURRICULUM VITA

Sergio Rafael Mendez was born May 30th 1987 in El Paso Texas. The second child of Sergio Rafael Mendez Nieto and Elvia Ortiz Garcia, he graduated from Hanks High School in the fall of 2004 and entered The University of Texas at El Paso the next semester. He received his bachelor's of science degree in Civil Engineering from The University of Texas At El Paso in May of 2010. He entered the Graduate School at The University of Texas at El Paso in the summer of 2010. While pursuing his master's degree, he worked as a research assistant at the Future Aerospace Science and Technology Center in The University of Texas at El Paso. He was an active member of the American Society of Civil Engineers student chapter and captain of the student steel bridge team since 2010. He is also a member of the Associated General Contractors and the Structural Engineers Association of Texas.

Permanent address: 1525 John Macguire
El Paso TX, 79912

This thesis was typed by Sergio Rafael Mendez